Physica 12D (1984) 83–106
North-Holland, Amsterdam

1.2. GASES

SHOCKS, INTERFACES, AND PATTERNS IN SUPERSONIC JETS

Larry L. SMARR†*
Departments of Astronomy and Physics, University of Illinois, Urbana, Illinois 61801, USA

and

Michael L. NORMAN and Karl-Heinz A. WINKLER
Max-Planck-Institut für Physik und Astrophysik, Institut für Astrophysik, 8046 Garching bei München, Fed. Rep. Germany

Supersonic gaseous jets exhibit coherent nonlinear dynamic structures. We use a supercomputer to obtain solutions to the equations of two-dimensional inviscid hydrodynamics, representing both axisymmetric and planar jets boring their way through a uniform medium. We use color images to display these high resolution computations. Several basic morphologies of interfaces and shock structures arise which we discuss in simple terms. The global structure of the two-parameter solution space is analyzed. A number of the basic structures, which appear in the supercomputer simulations, seem to occur in both terrestrial and astrophysical supersonic jets.

1. Introduction

Supersonic gaseous jets have been studied experimentally and theoretically for a century. Their scales vary from centimeters in the laboratory to millions of light years in radio galaxies. We briefly review their observed properties in section 2. A two-dimensional Eulerian hydrodynamics code is used to solve the dynamical evolution of a supersonic jet as it bores through a pressure confining medium. The numerical program is outlined in section 3. We explore in some detail the morphological patterns which occur in the axisymmetric case of matched jets, i.e. those in which the inlet pressure of the jet equals the exterior pressure of the confining medium. Color computer images are used to exhibit the physical properties of our solutions. In section 4, the existence of a cocoon of gas returning from the advancing head of the supersonic beam is shown to depend dramatically on the ratio of the beam density to the density of the surrounding medium: light hot beams have cocoons, while dense cold beams are naked. The Mach number of the beam, the other dimensionless parameter of our study, determines how mixed the cocoon becomes. Our numerical survey of solution space covers a factor of 1000 in density ratio and in beam luminosity. Shock systems are found to be ubiquitous in these jets. In section 5 we describe the various types of shocks which appear in the flow and show how they arise from unstable perturbations. We find that the nature of the shock systems is intimately coupled to the patterns of cocoon and beam discussed in the previous section. The stability of the interfaces in axisymmetric supersonic jets is examined in section 6. Again, the dynamics are dominated by nonlinear waves whose development depends on the density ratio and the Mach number. In section 7, we show how the shocks, interfaces, and patterns differ in slab jets. Finally, we conclude with some speculations about how fully three-dimensional jets will resemble our two limits of axisymmetry and planar symmetry. Throughout

†Visitor, Max-Planck-Institut für Astrophysik.
*Alfred P. Sloan Fellow.

0167-2789/84/$03.00 © Elsevier Science Publishers B.V.
(North-Holland Physics Publishing Division)

our study, our focus is on using the computer simulations to reveal the basic nonlinear structures which occur in the solutions of a fairly simple system of laws of physics. These nonlinear structures appear similar to many of the observed structures of terrestrial supersonic jets and are very suggestive as explanations of the knots and hot spots seen in astrophysical jets.

2. Real supersonic jets

The laboratory study of supersonic gaseous jets was begun a century ago by E. Mach and Salacher (1889) [1]. This work was extended by L. Mach, Emden, and Prandtl. What they discovered is illustrated in fig. 1, taken from the textbook on gas dynamics by Prandtl (1952) [2]. Here gas is shot through a small nozzle into the air. The nozzle pressure can be greater than (underexpanded jet), equal to (matched jet), or less than (overexpanded jet) the atmospheric pressure. The nozzle opening can be a long thin rectangle (slab jet) or a circle (axial jet). In any of these cases, a nearly periodic array of shock waves are found to be embedded in the flow. Fig. 1 is a matched slab jet photographed by Schlieren techniques, which rely on the rarefactions and compressions in the gas to modulate the illuminating light. If the Mach number is high enough, the intersecting shocks form a transverse Mach stem (in slabs) or Mach disk (in axial jets). For examples, see Landenburg et al. (1949) [3].

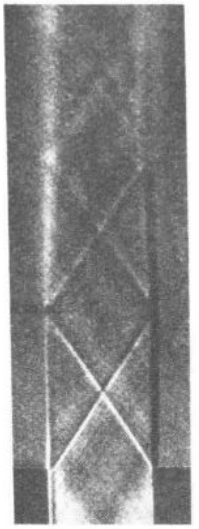


Fig. 1. A Schlieren photograph of the supersonic air flow emerging from a narrow slit. The long axis of the slit is into the page. The pressure in the inlet has been matched to the outside ambient pressure. There are a series of three crisscrossing shock waves standing in the flow. Notice that the jet/atmosphere interface is almost straight, even though there are large variations in the internal pressure caused by the shock waves. (From Prandtl, p. 285, 1952.)

In aerodynamics, the existence of these periodic internal shocks has been known since the beginnings of supersonic flight. Fig. 2 shows the supersonic exhaust plume from the Bell X-1 rocket plane, the first manned aircraft to break the sound barrier (taken from Anderson [4]). One sees the long axisymmetric jet with periodic bright and dark spots. The bright spots can be caused by either secondary recombustion of fuel in the high temperature regions following the internal shocks or by chemiluminescence [5].

In our galaxy, a growing number of astrophysical objects of roughly solar mass are being found to produce jets. Examples are: protostars (e.g. Mundt and Fried [6]), old binaries in supernova remnants (e.g. SS433, Margon [7]) and in planetary nebulae (e.g. R Aqr, Tapia et al. [8]). A number of these jets are knotty, see fig. 1 of Norman et al. [9], with the emission coming from high excitation atomic lines.

Finally, an enormous number of jets have been discovered in the last few years emerging from the centers of galaxies and quasars. Here the primary energy source is assumed to be accretion onto a supermassive black hole of 100 million solar masses. The focusing of that energy into two oppositely directed jets occurs either near the hole (see the review by Blandford [10]) or in the galactic atmosphere (Smith et al. [34]). The jets range in size from thousands to millions of light years in length, with a typical length of 50–100 jet diameters. Many of these jets exhibit knots of emission internal and external to the beams. Fig. 3a shows a well-studied example of internal knots, NGC 6251 (Perley, Bridle, and Willis [12]). In several cases, e.g. M87 and Centaurus A, these internal knots are

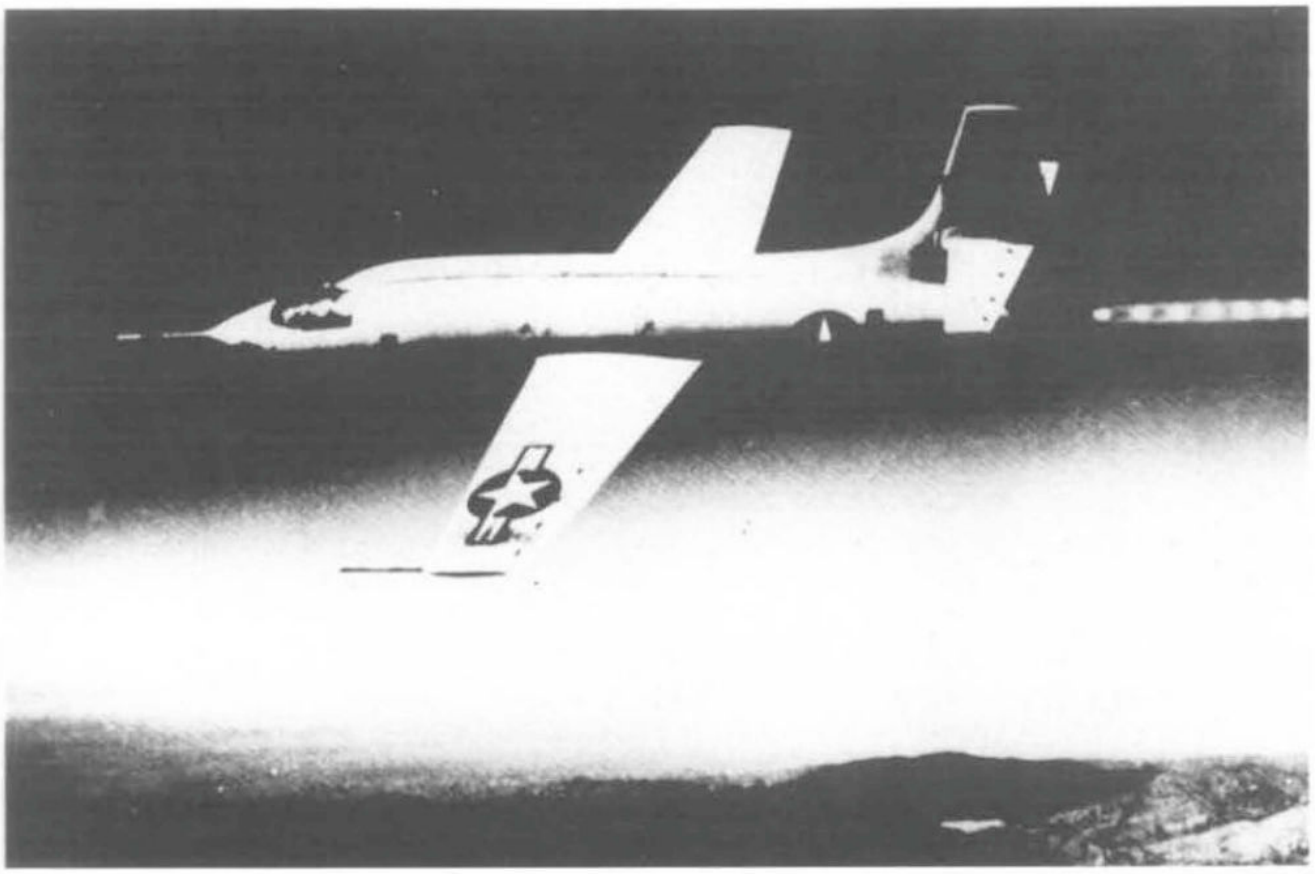


Fig. 2. The supersonic exhaust plume from the rocket plane Bell X-1, the first manned plane to break the sound barrier. Note the periodic bright emission knots in the exhaust beam, with spacing about two beam diameters. There are at least six of these knots, which are caused by secondary combustion of fuel as the exhaust gas moves through the embedded series of crisscross shocks. Again note that the jet diameter is essentially constant even though there are strong internal shocks. (From Anderson, 1981).

seen in all wavelengths from radio to X-ray. The *internal* knots are caused by synchrotron emission from electrons, shocked up to high energy, spiraling around a local magnetic field. The *external* knots (e.g. Miley [13]) are similar to the stellar jets in showing high excitation atomic lines.

In addition to the knotty beam, the advancing head of the jet can be seen in many extragalactic jets. The beam ends in a characteristic "hot spot", usually embedded in an amorphous lobe of emission. Again, the emission is synchrotron radiation. Fig. 3b shows a typical example (3C111 taken from an observation of Perley, see Fomalent [14]). There one can see another feature which often occurs. Although the jet is remarkably straight, the jet begins to bend toward the end, making the knots and hot spots appear slightly off the center line of the jet.

In summary, the observations of supersonic jets point to a very similar underlying hydrodynamics flow. The beams appear to preserve their initial symmetry (planar or axial) for many beam diameters downstream. The opening angles are usually small, indicating that the supersonic flow preserves collimation unless the external pressure is suddenly altered (Sanders [15]). In most cases, the external gas pressure seems to be the confining agent, although in some cases magnetic fields may be necessary. Knots of higher pressure, density, and temperature, caused by internal shocks, seem

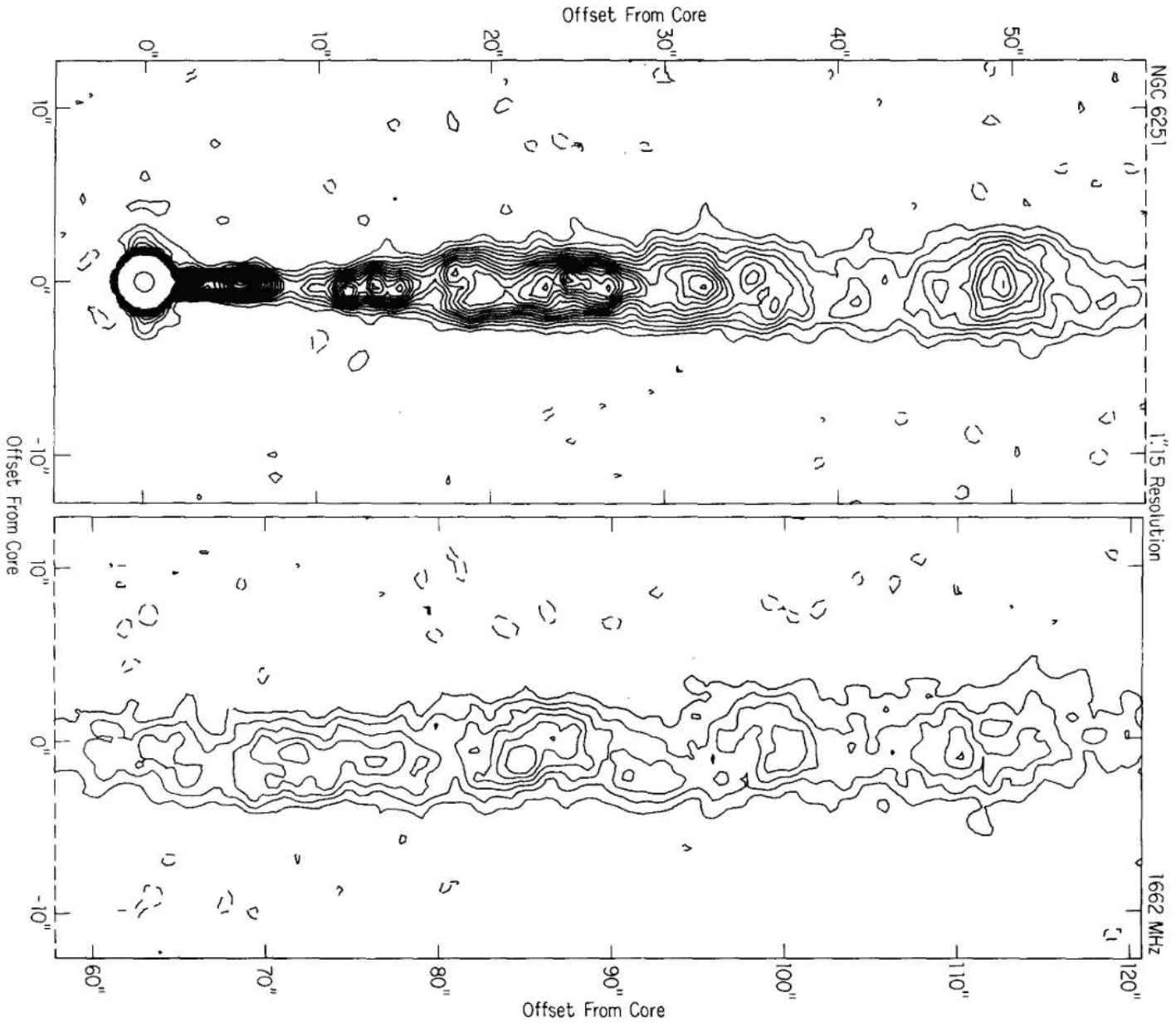


Fig. 3. Examples of astrophysical supersonic jets. Fig. 3a. A high resolution radio interferometric map made with the Very Large Array of radio telescopes in Socorro, New Mexico. This map details a portion of the inner jet of the radio source associated with elliptical galaxy NGC 6251. One can see that the emission is knotty along the beam. The circular feature at 0″ is the center of the radio galaxy. The map has been broken into two sections (0″–58″, 58″–120″). The distance scale is that 10″ = 22 light years. The piece of the jet shown is therefore 260 light years = 2×10^{18} meters in length (reprinted by permission of A. Bridle and R. Perley).

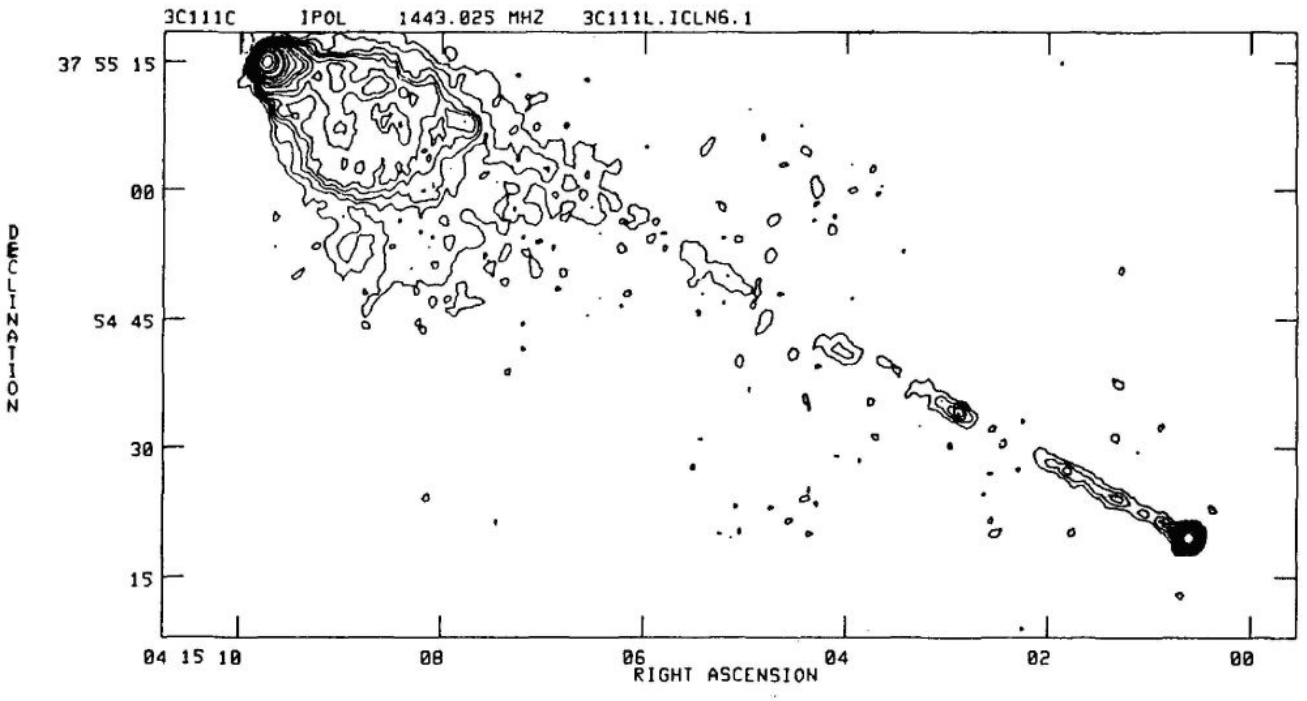


Fig. 3b. A VLA map of radio source 3C311. The contours are of total radio intensity at 1.4 GHz. Note the long knotty linear jet ending in a hot spot at the end of a lobe of amorphous emission. The circular feature at the lower right-hand of the map is the center of the radio galaxy (reprinted by permission of R. Perley).

to be ubiquitous in the supersonic beams. These internal shocks typically do not disrupt the beam, however the very strong shock at the head of the beam (the "hot spot") does terminate the flow. The head of the beam is often embedded in an amorphous lobe and indeed the beam itself is often surrounded by a "cocoon" of low surface brightness emission. Finally, the jets seem remarkably stable. The shear layers on the surface of the jets are subject to Kelvin–Helmholtz instabilities, which can grow to nonlinear amplitude. The large wavelength instabilities (pinching and kinking modes) threaten global beam stability, while small wavelength instabilities should lead to turbulent mixing. In spite of this, supersonic jets are able to propagate to large distances.

To supplement the data obtained from laboratory experiments and astrophysical observations, we have performed high resolution supercomputer simulations of the interior of the supersonic beam, its surroundings, and the entire length of the jet from the near-inlet region out to the advancing head. This provides an appropriate set of solutions to the compressible gas dynamics equations from which we can study whether observed properties of jets naturally develop as nonlinear phenomena in supersonic flow. The enormous volume of "data" produced by the supercomputer is first reduced graphically. Then simple models are devised which can explain many of the morphologies seen in the computer images. This approach thus provides a new tool to the century old research effort to understand supersonic jets.

3. Computational supersonic jets

Our use of computers to solve a basic physics problem follows the strategy foreseen many years ago by John von Neumann. This approach was

recently paraphrased by the mathematician Garett Birkoff:

> ...it seems clear that von Neumann was envisioning fluid dynamics as a *mathematical science*, as had Euler, Lagrange, Stokes, Riemann, and Poincaré before him. His main point was that mathematicians had nearly exhausted *analytical* methods, which apply mainly to *linear* differential equations and *special geometries*... In short, von Neumann's proposal was that, with large scale, high speed digital computers, one could substitute *numerical* for analytical methods, tackling *nonlinear* problems in *general* geometries.
>
> SIAM Review 25 (1983) 1.

Our program is to solve the basic equations (mass continuity, Euler equation, energy equation) of inviscid compressible hydrodynamics for a well-posed physics problem and see what features of the solutions can be understood a posteriori in simple terms. This approach follows in a direct way the synergetic method, described by Zabusky [17], which was used in the discovery of the properties of solitons which arise in nonlinear dispersive equations. Even though our solutions are much more complicated, they will turn out to possess features in common with many of the solutions of the other nonlinear equations discussed in these proceedings.

There are a number of important advantages to using a computer to obtain solutions to a complicated physics problem. First, one can control precisely which laws of physics are operating. In both observation and experimentation, one is dealing with a variety of physical effects which may be difficult to sort out. An example is the difficulty in producing a truly inviscid flow in the laboratory. With the computer one can see which phenomena emerge from the inviscid hydrodynamics, then carefully add in viscosity, magnetic fields, etc. and see how that alters the solutions. Second, one has complete control over the environment of the solution. It is simple to produce gradients in the background pressure or change from atmospheric to interstellar pressures. Third, one can explore how the solution space phenomonology changes as one varies the fundamental parameters of the problem. Fourth, one can compute over a much greater dynamical range of parameters than can be done in the laboratory. To go from a dense jet to a light jet requires only the change of an input statement, not building a new laboratory apparatus. Finally, modern color computer image techniques allow one to read out in great detail any physical variable of interest. In many cases, the only observables in experiments or observations are complicated combinations of the basic physical variables.

Unfortunately, computers are still not fast enough with large enough memories to handle general 3-dimensional dynamic flows at sufficient resolution to describe jet physics. However, they are quite capable of resolving two spatial dimensions. The solutions we present here use a large fraction of the central memory of a CRAY-1 supercomputer and require between one and thirty hours of CPU time per evolution. We compute both axisymmetric and planar symmetric jets. The computations and graphics were done at the Max-Planck-Institut für Physik und Astrophysik, Institut für Astrophysik, in Garching b. Munchen, West Germany.

The code we use for solving the equations of gas dynamics is described in Norman and Winkler [18]. It is a time explicit, Eulerian, finite differenced code with interface trackers, which has been extensively calibrated on many problems. The advection is by van Leer's monotonic method. There were two sets of axisymmetric evolutions which we performed. The first set (completed in 1981) used a grid which was 30 jet radii long and 7.5 wide. The supersonic beam had 8 zones across its radius. The second set of runs (made in 1982–83) used the same resolution but extended the grid to 80 jet radii in length and used a ratioed zoning from 7.5 out to 15 jet radii in width. The

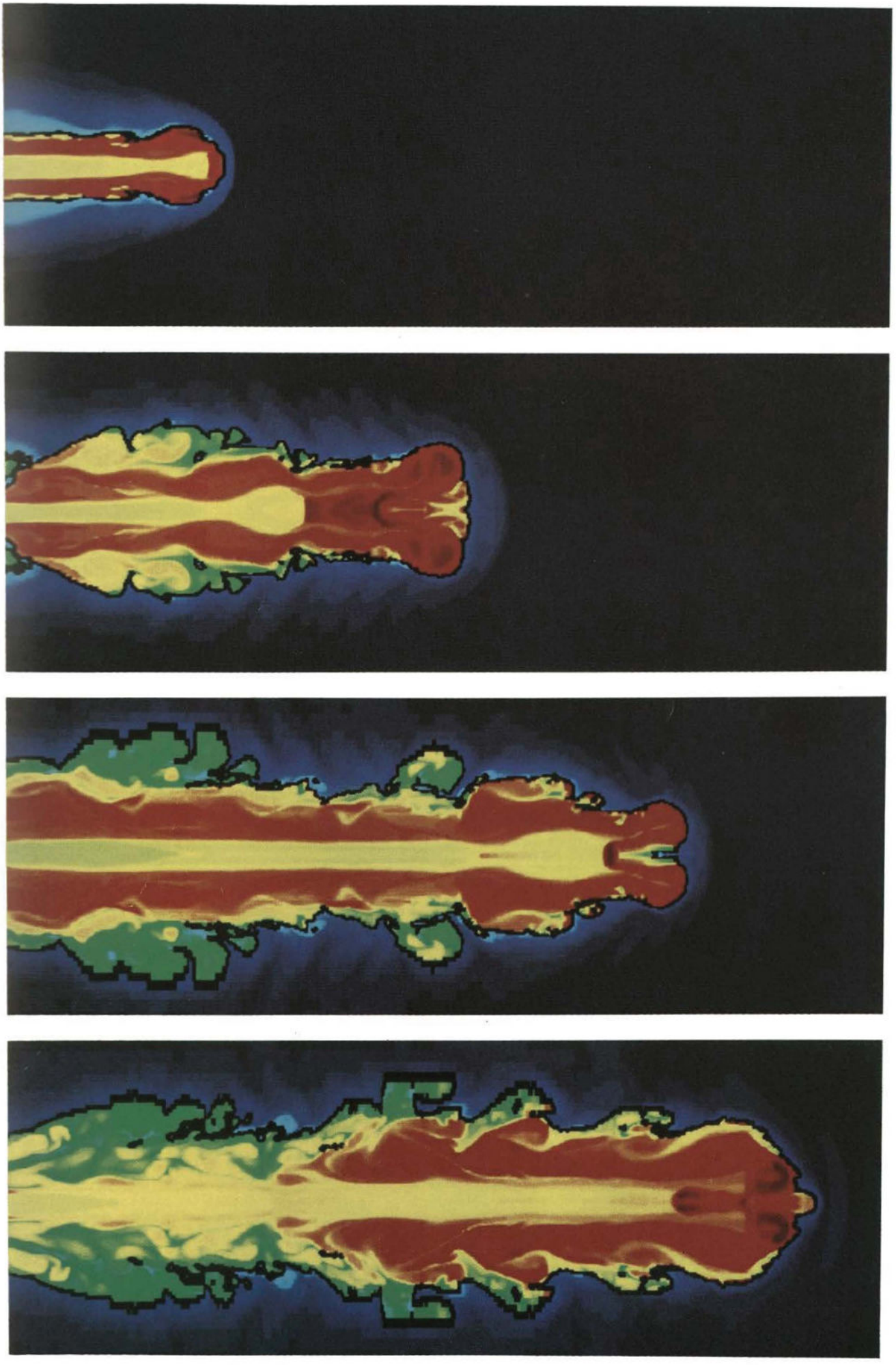


Fig. 4 (for caption see text following this set of color plates).

planar jets were run on a Cartesian grid with 20 equidistant zones across the jet and 70 ratioed zones on either side of the jet. The grid was 300 zones long. In all cases, gas of a specified Mach number (initial velocity of beam gas in the lab frame divided by the internal sound speed of the beam gas) and density ratio (of beam gas divided by ambient density) was shot into the grid and allowed to propagate through a uniform gaseous ambient medium. In most cases the inlet pressure in the jet equaled the ambient gas pressure so that a matched jet resulted. We have assumed a perfect gas law for both beam and ambient gas, with the ratio of specific heats in each gas equal to 5/3.

The results of the first set of runs were reported in paper I (Norman et al. [19]). The propagation and morphology of the second run of jets was graphically presented (in grey tones) in paper II (Norman et al. [20]). An in-depth discussion of the internal shocks and the resulting knots was given in paper III (Norman et al. [9]). The comparison of the terminal strong shock with astrophysical hot spots was made in paper IV (Smith et al. [11]). As stated above, the code itself was documented in paper V (Norman and Winkler [18]), while the new color image algorithm was given in paper VI (Winkler [21]). This paper can be considered a summary paper in which we focus on the generic nonlinear structures we discovered in this project. It will also serve as a comprehensive documentation of the solution space of the axisymmetric jet problem.

4. Patterns in axisymmetric jets

As the supersonic gas emerges onto the grid, it drives a bow shock ahead of itself. The boundary of the jet gas with the ambient gas is a contact discontinuity. Since in general this contact will propagate more slowly than the gas in the supersonic jet beam, a shock will form behind the contact which both stops the beam gas before it hits the contact and deflects the gas out of the beam. This much of the structure of the advancing head of the jet was reasoned out in the landmark paper on astrophysical jets by Blandford and Rees [22].

In fig. 4, one can see all these features in four snapshots of the evolution of a Mach 6, density ratio 0.01 jet. The color at any point represents the intensity level of the quantity being plotted, with dark blue being the lowest value and bright red being the highest value. The order of the colors is that of the spectrum (see color bar in fig. 6). There are 73 increments in color space, each representing an equal logarithmic increment in the quantity plotted. Thus, our color bar spans the entire dynamic range of the physical quantity plotted. Since our grid has 640 grid points along the axis of symmetry, while the color image has only 512 pixels, the image slightly underresolves our solution. The physical values are those in a plane of symmetry which contains the axis of rotation. Because of the assumed axisymmetry, the calculation need only be done in the upper half plane, but we have plotted the image with both half planes.

The physical quantity represented in fig. 4 is entropy. As the jet propagates, the inner beam maintains a fairly constant entropy (yellow) which is much higher than the cold ambient gas (dark blue). The beam is terminated in a strong shock where the entropy jumps from yellow to bright red. This termination process is geometrically complex and time dependent. This dynamics is intimately related to the development of the regularly spaced surface waves, which one can see generated in fig. 4. These waves are on the interface between the return gas flow (the cocoon) and the ambient medium. These breaking waves, combined with the swirling red color in the entropy under the waves point to the existence of large scale vortices in the cocoon flow. These vortices are responsible for mixing the low entropy gas from the ambient medium into the high entropy shocked gas in the cocoon leading to the well mixed yellow and then green of the entropy further downstream. One can repeat this process of

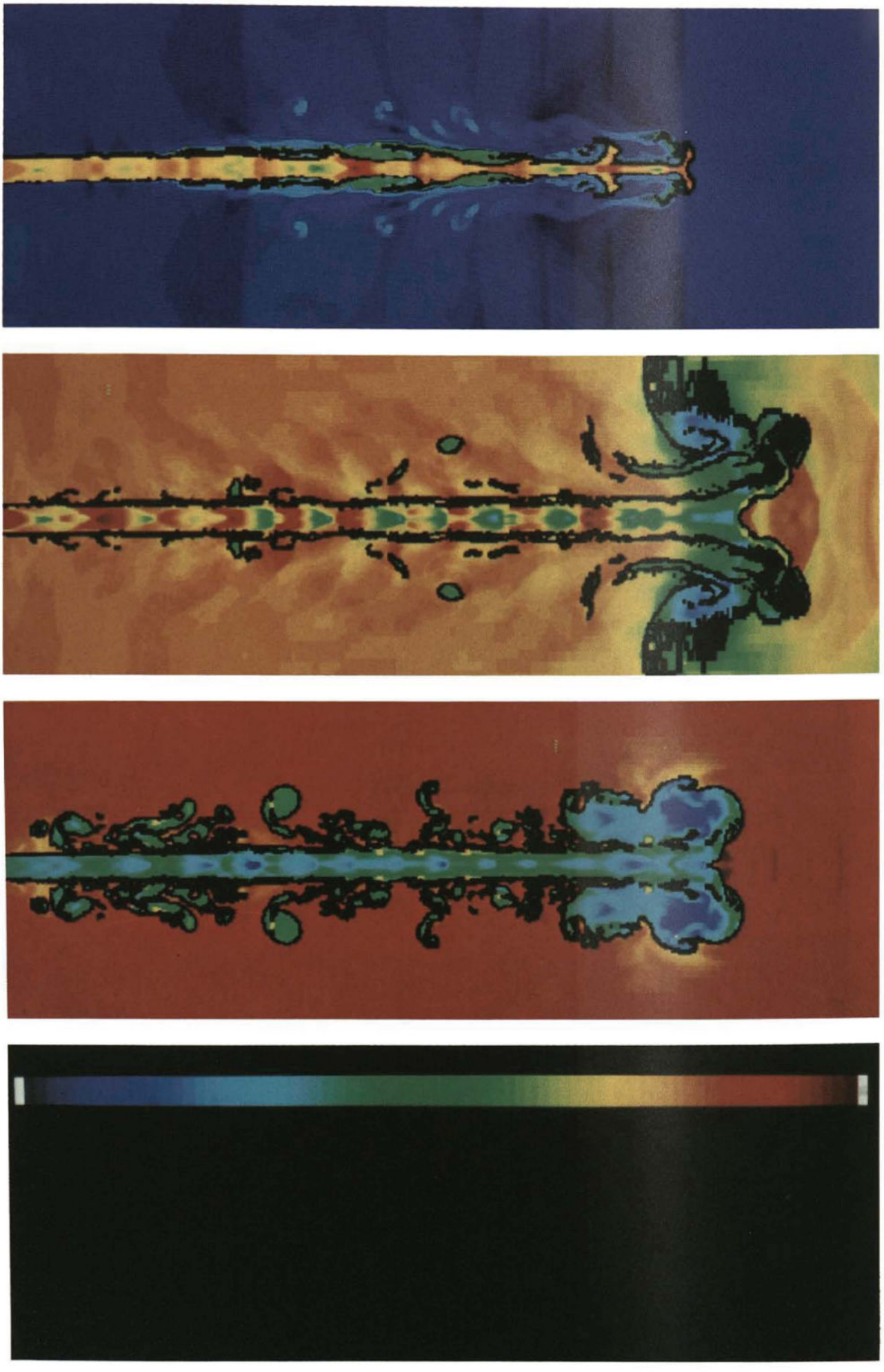


Fig. 6a (for caption see text following this set of color plates).

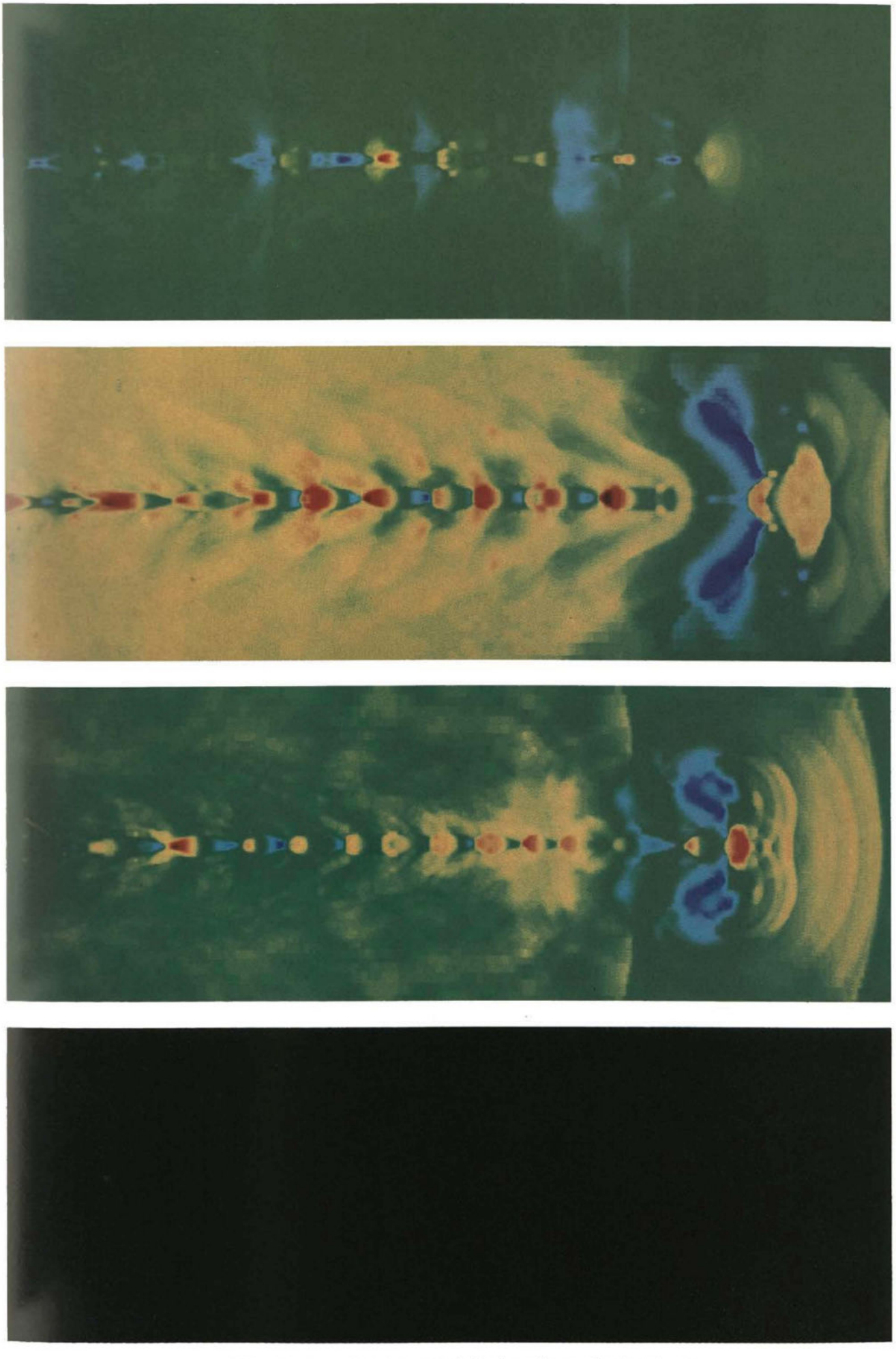


Fig. 6b (for caption see text following this set of color plates).

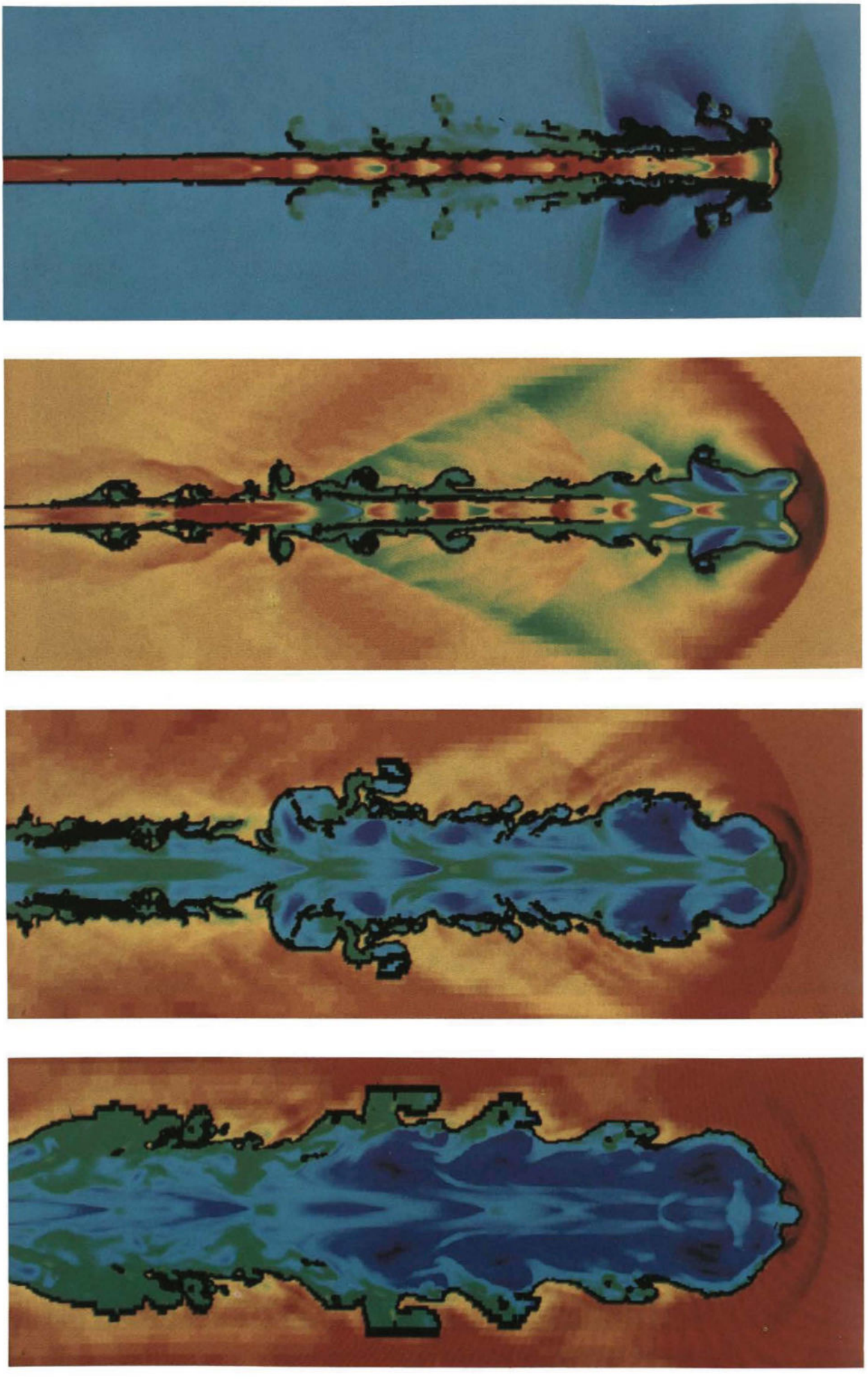


Fig. 7a (for caption see text following this set of color plates).

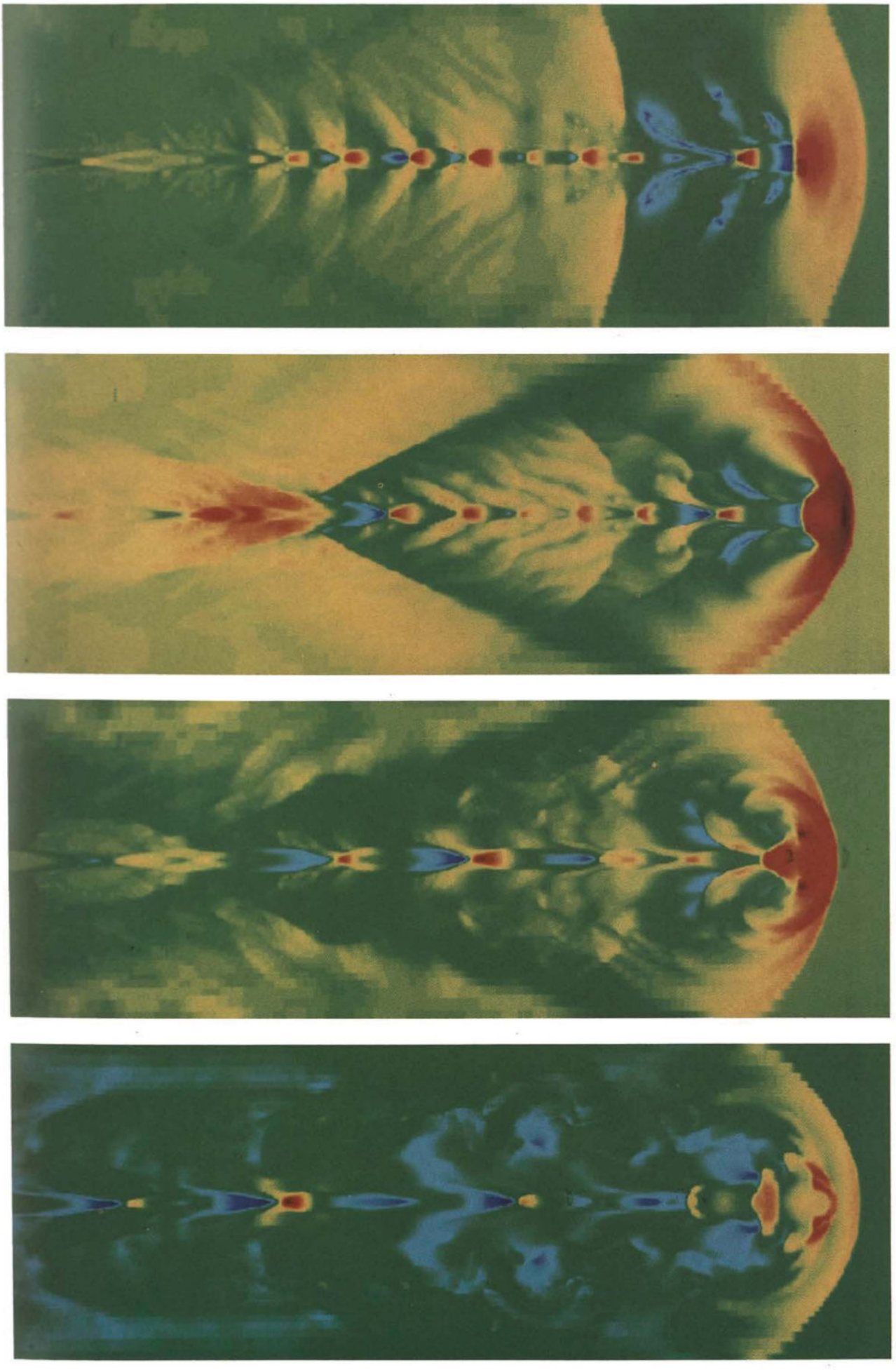


Fig. 7b (for caption see text following this set of color plates).

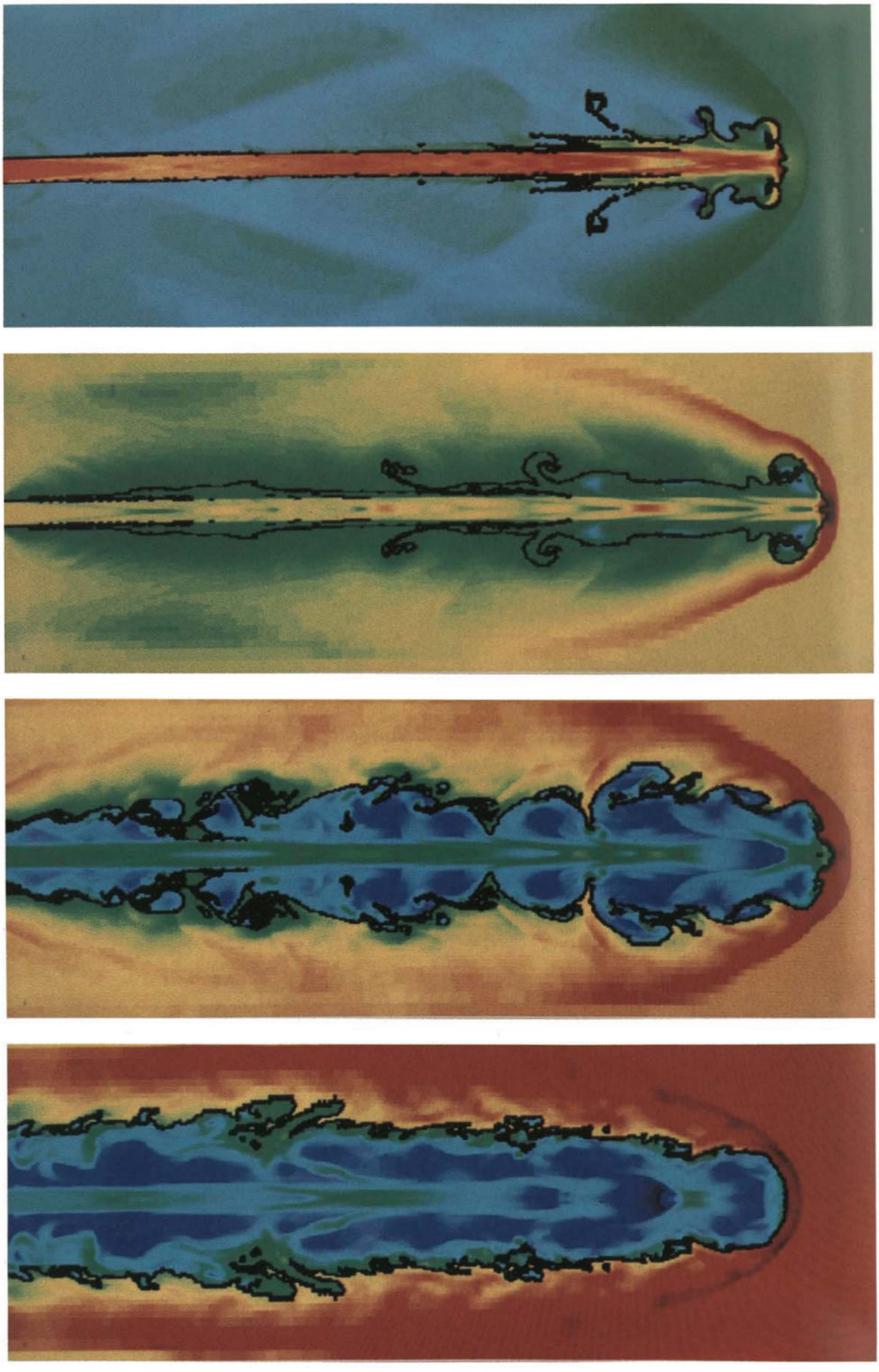


Fig. 8a (for caption see text following this set of color plates).

unraveling the physics of jet propagation, by studying the evolution of each of our axisymmetric jets pictured in grey scale images in paper II.

The evolutions we ran are located in the Mach number–density ratio plane as shown in fig. 5. In this paper we concentrate on four different density ratios (0.01, 0.1, 1, and 10) and three different Mach numbers (3, 6, and 12). We do not study in any detail the Mach 1.5 jets which we have also computed, because we believe that such low Mach number jets are so unstable to nonaxisymmetric modes that our axisymmetric computations are not relevant to the real world. The dynamic range of our sample is then 1000 in density ratio. Since the dimensionless kinetic energy luminosity scales as (density ratio)$^{-1/2}$ (Mach number)^3, then (see fig. 1 of paper II) a Mach 12, density 0.01 beam is 2000 times as luminous as a Mach 3, density 10 beam.

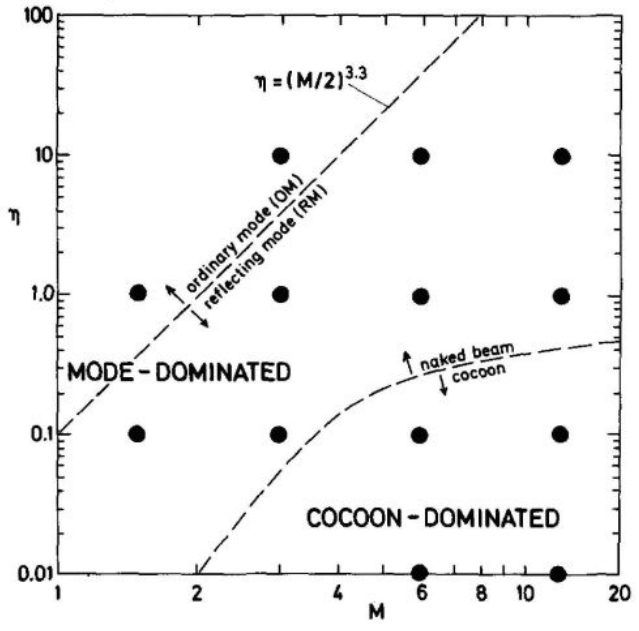


Fig. 5. The two-parameter space of pressure matched supersonic jets. The vertical axis is the log of the density ratio between the inlet gas and the ambient medium. The horizontal axis is the log of the internal Mach number of the inlet gas. The heavy black dots are the jets we have calculated. The jets have a cocoon of return flow below the curved dashed line; they have only a naked supersonic beam above it. These jets are called mode-dominated if the jet is naked and cocoon-dominated if not. All of the jets develop internal shocks. The shocks are planar and disruptive if the jet lies above the straight dashed line; they are biconical and nondisruptive if they are below the line. The equation for this dashed line comes from Cohn's 1983 study of linear perturbations of axisymmetric jets.

We present in figs. 6, 7, and 8 a picture album of the morphology of the solution space for these two parameters. The color graphics scale is as above. Each page represents jets of the same Mach number, with the densest jet (density ratio 10) at the top, and the lightest jet (density ratio 0.01) at the bottom. The images are snapshots of each evolution taken at a time (table I) in which the jet has reached a length of ~ 75 jet radii. Facing pages are the same jets with their density field plotted on one page and its pressure field plotted on the other page. The numerical values of the maximum and minimum density and pressure for each jet shown are given in table I.

The reason for showing both pressure and density is twofold. First, the density plots show very

Table I
The quantitative data for the jets shown in figs. 6, 7, and 8. The units of time, density ratio, density, and pressure are fixed by the ambient medium values. The radius of the jet inlet is taken to be 1, the sound speed in the ambient medium is 1, the time unit is the time it takes the external sound speed to cross the jet radius, the external density is 1, the external pressure is 0.6 (since the ratio of specific heat is 5/3). The Mach number is the ratio of the inlet velocity to the internal sound speed of the supersonic beam. The density ratio is the inlet beam density in units of the external medium density

Mach Number	Density Ratio	time	ρ_{min}	ρ_{max}	p_{min}	p_{max}
3	10.0	95	4×10^{-1}	18	0.13	2.0
	1.0	100	5.3×10^{-2}	1.4	0.03	1.2
	0.1	60	9.7×10^{-3}	1.7	0.06	3.2
6	10.0	60	3.1×10^{-1}	19.0	0.08	2.5
	1	34	7.6×10^{-2}	2.4	0.03	3.3
	0.1	27	6.7×10^{-3}	3.3	0.01	7.8
	0.01	26	9.6×10^{-4}	3.4	0.04	13
12	10.0	28	1.4×10^{-1}	25	0.03	6.0
	1.0	14	2.3×10^{-2}	5.7	.03	32
	0.1	10	4.0×10^{-3}	5.4	0.02	64.
	0.01	7.6	4×10^{-4}	4.0	0.04	50.

clearly the location of contact discontinuities, which are interfaces in pressure equilibrium. These discontinuities often have large jumps in density across them, but they are invisible in the pressure plots. Second, the pressure plots are much more sensitive to the strength of shocks than density plots. The jump in density across a strong planar shock saturates at four, while the jump in pressure across a shock continues to rise with the shock strength. By comparing the two plots for each jet, one can infer most of the important physics of the flow.

The most obvious pattern that one sees in these plots is that the cocoon rapidly disappears as one goes from light to dense jets. Futhermore, if one keeps the density ratio fixed, one gets more cocoon as one increases the Mach number. As discussed in detail in papers I and II, there are several effects which cause these trends. First, energy and momentum balance, applied in a frame moving with the bow shock, tells one that a light, low inertia, jet will bounce back from its collision with the dense ambient medium, thus producing a large backflow in light beam jets. A similar argument predicts that when dense beam gas is halted in the frame of the head of the jet, its inertia will keep it moving with the bow shock, thus creating no appreciable backflow for dense jets. Second, as the Mach number of the beam increases, so does the Mach number of the backflow. This raises the relative Mach number of cocoon/ambient medium interface, which stabilizes it against the disruptive Kelvin–Helmholtz instability. Finally, we are comparing our jets at fixed length, not at fixed time. For those jets with lower Mach number, not only is this interface more unstable, but there have been more eddy turnover timescales in which to disrupt the cocoon, than in the faster moving high Mach number jets.

Another pattern one sees is that the location of the pressure maximum varies considerably with the parameters. It can be either located between the bow shock and the shock which terminates the flow ("hot spot dominated" jets), or it can be in the beam itself, often appearing as a quasiperiodic set of maxima ("knot dominated" jet). The jets become more hot spot dominated as the Mach number increases, since the strength of the bow shock, and therefore the pressure jump across it, increases with the Mach number. In the following sections, we will study this set of solutions in more detail. Our aim will be to draw out general properties of such flows and explain them in simple terms.

5. Shocks in axisymmetric jets

By solving the full nonlinear dynamic equations, one can determine the global structure of shock systems in these jets. We have discovered that there are three major classes of shocks: those which are internal to the beam, those which are external to the beam, and those which terminate the beam. Since each class will have observational signatures, particularly in astrophysical jets, we will discuss the patterns which we have found in each class.

We illustrate the different shock structures by considering in more detail two of the Mach 6 jets, the density ratio 10 and 0.01 cases (top and bottom jets in fig. 7). In figs. 9a and 11a, we exhibit $\nabla \cdot V$, the scalar convergence (dark grey) and divergence (light grey) of the velocity field for the two jets at the same times as shown in fig. 7. These dark and light grey regions plotted represent the most extreme volumes of compression and rarefaction, respectively. In both the dense and light jet cases (figs. 9a, 11a), the supersonic beam has alternating regions of rarefaction and compression. These show up as low (blue/green) and high (yellow/red) pressure regions, respectively, in fig. 7. The compression zones occur across shock fronts, where the velocity suffers a discontinuity. The sharpness of the compression zones indicates the resolution of the shock waves in our code. The strength of each shock or rarefaction can be judged

by looking at the color pressure plot to see what jump in pressure occurs across each feature.

5.1. *Mode dominated internal shocks*

Fig. 9a illustrates a mode dominated beam; here a regularly spaced pattern of shocks occurs in the beam. This induces a quasiperiodic string of high pressure knots along the beam as seen in fig. 7. We have explored this regime in depth in paper III. We find that these jets do not have extensive cocoons around the beam. As a result, the unstable

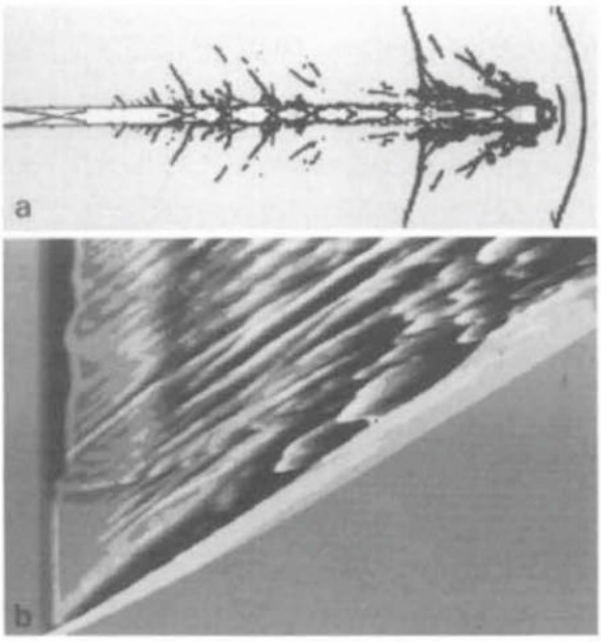


Fig. 9. Shock structure of the Mach 6, density ratio 10 jet. The top image (a) shows regions of extreme compression in black and extreme rarefaction in gray. The sharply defined compression regions delineate the shock waves in the flow. There are external shocks in ambient gas and internal shocks in the beam. One can see the characteristic "x" shape of the internal biconical shocks. The lower figure (b) is a spacetime diagram of the pressure along the symmetry axis. The horizontal scale is space and the vertical axis is time. The maximum value of pressure is white, the minimum is black, and the intermediate values are 15 shades of grey representing equal logarithmic intervals of pressure between the maximum and the minimum. The shocks are located where the tone abruptly changes from dark to light. One can see that the periodic internal shocks propagate at the same velocity as the bow shock. The shocks preserve themselves as they propagate, with new shocks appearing behind them as they move downstream.

axisymmetric modes predicted by the linear theory of the Kelvin–Helmholtz instability (Hardee [23–25]; Ferrari, Trussoni, and Zaninetti [26, 27]; Ray [28]; Cohn [29]), as applied to the naked beam/ambient medium interface, can grow freely. The linear theory can accurately estimate the growth length of the instability, i.e. how far down the beam the instability is advected before it has grown to nonlinear amplitude. This length scales as the Mach number. This is why the dense Mach 12 jets in fig. 8 without cocoons do not show knots – the beam moves so fast that the instability has not had time to become nonlinear. If the Mach 12, density ratio 10 jet is evolved further (fig. 11 of paper III), the knots appear looking much like the Mach 6, density ratio 10 jet in fig. 7.

What the linear theory cannot predict at all is the nature of the final saturated nonlinear state. As can be seen by viewing Figs. 6 and 7, the unstable surface perturbations saturate by creating shock waves across the beam. The shocks are planar if the Mach number is low enough and the density high enough (above the straight dashed line in fig. 5). Of the jets studied in this paper, only the Mach 3, density ratio 10 jet (fig. 6) is in this regime. Note that these shocks disrupt the beam, causing it to neck down severely. Below this line in fig. 5, the shocks appear as "x's" (biconical in our axisymmetric geometry) and they do not disrupt or pinch off the flow.

The dividing line between planar and biconical shocks, discovered in our numerical survey, coincides closely with the line discovered in the linear theory (Cohn, [29]) which divides the unstable jets into those in which the ordinary mode (OM) is most unstable and those in which the reflecting mode (RM) is most unstable. The difference between these two modes is that the OM is homogeneous across the beam, whereas the RM has internal nodes in the beam. We hypothesize that the homogeneous OM's lead to planar shocks and the RM's with one node lead to a biconical shock. We have begun making high resolution computations on "clean" beams to verify this hypothesis (see, e.g. fig. 9 of paper III).

The spacing of the knots depends only slightly on Mach number. We find that it varies between 2.3 and 2.6 jet diameters. These knots are not stationary in space, but propagate with a well-defined pattern velocity. This can be graphically seen in fig. 9b, which is a spacetime diagram of the pressure along the symmetry axis. The maximum value of pressure is white, the minimum is black, and the intermediate values are 15 shades of gray representing equal logarithmic intervals of pressure between the maximum and the minimum. The shocks are located at the places where the shade goes abruptly from black to white. The vertical axis is time, while a horizontal slice through the diagram gives the pressure profile on the spatial axis at that instant. The line at about 45 degrees is the bow shock advancing through the ambient medium.

One sees that the pressure knots have a remarkably parallel spacetime flow. New shocks appear behind the older ones as the older ones move downstream. Thus the nonlinear knot structure has a well-defined spacing and pattern velocity. This figure illustrates the power of computer graphics to highlight the physics of interest in dynamic nonlinear systems, just as Zabusky [17] has argued in the much simpler problem of the one-dimensional nonlinear dispersive equations.

To quantify the knot structure, we present graphs of the key physical variables on a cut along the axis of symmetry (fig. 10a). One can see that although the velocity remains fairly constant along the jet, the other properties of the jet are very inhomogeneous. For instance, the Mach number varies from 3 to 10 and the density from 2 to 15. These large variations are caused by the internal shocks in the beam. Note that because these are not planar shocks, the density jump across the shock can be greater than 4. Although these internal shocks are strong, they do not cause the jet to become subsonic, in the ambient medium frame, until the terminal shock.

This set of graphs illustrates the conceptual difficulty in applying perturbation theory to supersonic phenomena. The perturbation theory must assume a smooth stationary background to perturb around. However, precisely because the flow is unstable, the self-consistent background is unsmooth and unstationary. Therefore, the interpretation of perturbation theory, in the absence of fully nonlinear calculations, must be treated with caution.

In fig. 10b, we make a cut at right angles to the beam at a distance of 45 units down the symmetry axis. The boundary of the beam is sharply defined by the kinetic luminosity plot. Note that there is no appreciable backflow (negative V_z) surrounding the beam. The dip or peak at the center of the beam occurs because we have chosen a cut through one of the "x" shocks. The cut is made just forward of the center of the "x" so that the axis has been shocked, while the off-axis flow has not been. Thus, the axis is temporarily at high pressure compared to the edge of the beam. These graphs show that very large *transverse* pressure gradients occur in supersonic jets, in addition to the large jumps in pressure *along* the beam. Nonetheless, the beam diameter stays almost constant along the jet.

5.2. *Cocoon dominated jets*

The internal shocks in the supersonic beam divide the jets into two broad subcategories: the mode dominated (fig. 9) and the cocoon dominated (fig. 11) jets. The boundary in parameter space between these two domains is not sharp, but is estimated by the curved dashed line in fig. 5; it represents the division between those jets which have cocoons and those which do not.

We now turn to the cocoon dominated regime of low density, high Mach number jets, which possess strong backflows. A representative example is the Mach 6, density ratio 0.01 jet shown in figs. 7, 11, and 12. The spacetime diagram (fig. 11b) shows that the mode dominated shocks do not exist here. Instead, there is a slow backward drift of large regions of low and high pressure separated by shocks; (note that the vertical timescale is not the same as in fig. 9b). The beam

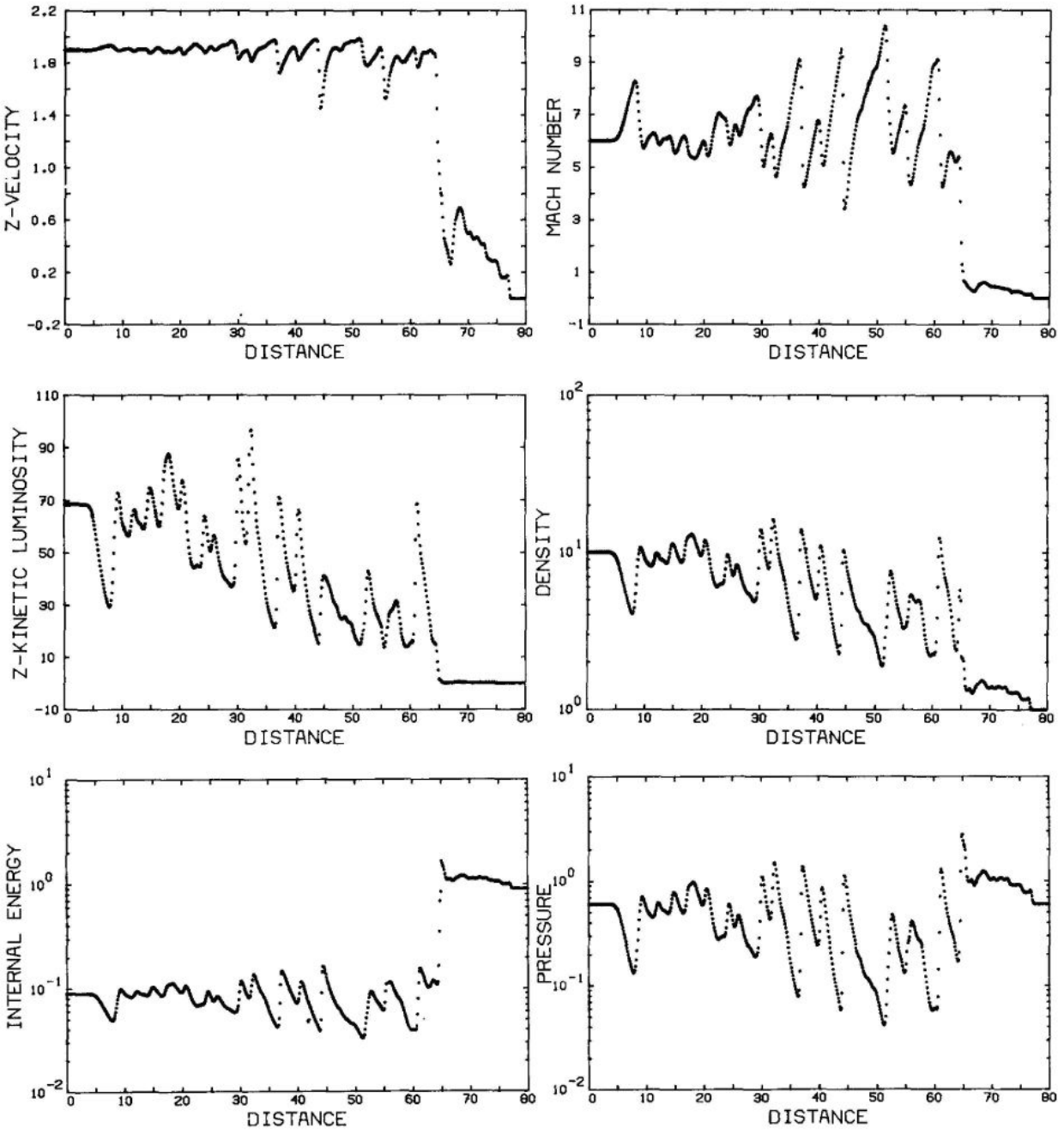


Fig. 10a. Physical variables along the symmetry axis (Mach 6, density ratio 10). Shown are the velocity (V_z), the internal Mach number (M), the kinetic luminosity (ρV_z^3), the density (ρ), the specific internal energy or temperature, and the pressure. Note how inhomogeneous the beam is. The quasiperiodic internal shocks cause the abrupt jumps. The dots are the grid points used in the computer simulations. The distance is in units of the beam radius.

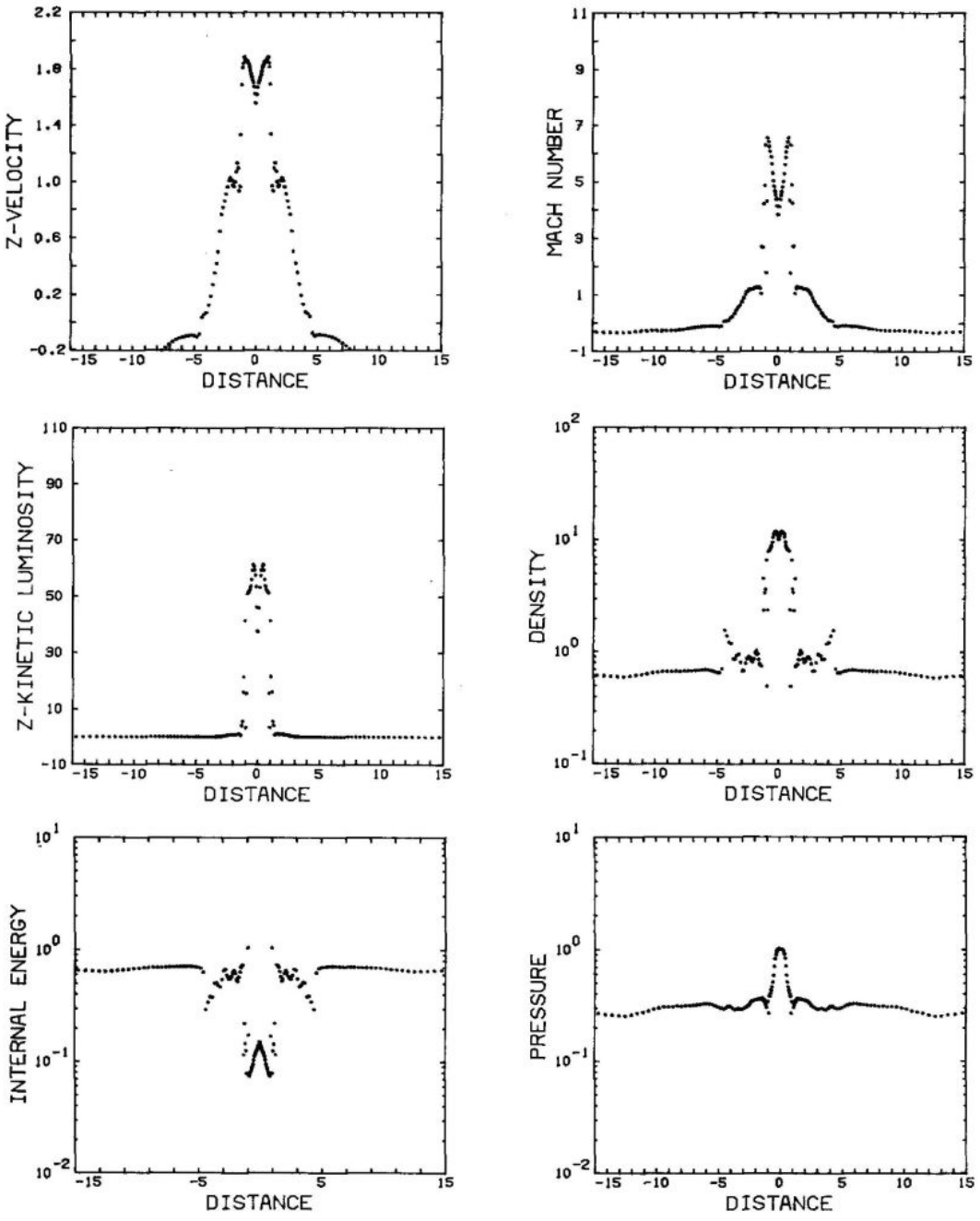


Fig. 10b. Same as 10a, except the cut is across the jet at $Z = 45$ units. The location of the beam is seen by the abrupt falloff in the kinetic luminosity. Note that the beam is still the same diameter as when it left the inlet. The peak or valley at the center of the beam occurs because the cut goes across one of the "x" shocks embedded in the beam.

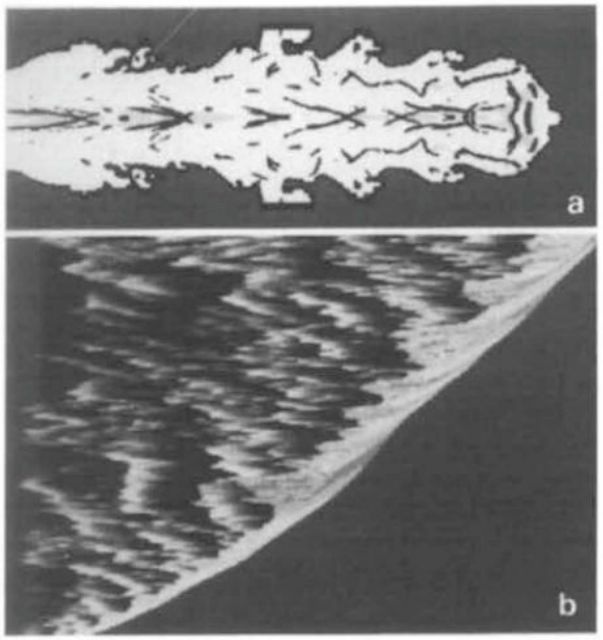


Fig. 11. Same as Fig. 9, except for the Mach 6, density ratio 0.01 jet. The shocks external to the beam are in the cocoon rather than the external medium. Note that they sometimes smoothly connect with the internal shocks. Even though the internal shocks are forced by the cocoon, they are biconical just as the free shocks in fig. 9. The terminal shock system is complex, but part of it is a strong Mach disk which stops the beam. The pressure spacetime is totally different than in the mode-dominated jet in fig. 9. The shocks which were part of the terminal shock system are left behind when the vortices are shed. These shocks gradually drift backward with the vortices. This shows that the shocks are pinned by cocoon physics and are not the free modes of a naked beam. The time-scale is about one half of that in fig. 9, since the light jet advances at about twice the speed of the dense one.

shocks are still biconical, but they start outside of the beam in the cocoon (fig. 11a). The spacing between shocks is much longer than in the mode dominated case, being roughly equal to the spacing of the large "breaking waves" seen on the interface between the cocoon and the ambient medium. These vortices sit in the cocoon, imposing pressure variations along the surface of the beam, which in turn, forces shocks into the beam.

In fig. 12a, we give the physical variables along the axis. We notice the fundamental effect, that the beam is broken up by biconical internal shocks, is present here as in fig. 10a. However, the spacing, while still fairly regular, is much larger than in the mode-dominated case. This is because the spacing in fig. 12a is set by the spacing of the forcing vortices in the cocoon, whereas the spacing in the mode-dominated case is set by the most unstable reflecting mode of a "free beam". The spacing of the cocoon vortices is ultimately set by the vortex shedding instability of the head of the jet.

Even though both jets (figs. 10a and 12a) start with Mach 6 inflow, the velocity of the light jet is $(1000)^{1/2} \sim 31.6$ times higher than the heavy jet. This is because both jets are in pressure equilibrium with the same ambient medium. As the density of the heavy jet is 1000 times that of the light jet, the temperature (see internal energy graphs in figs. 10a and 12a) of the light jet is 1000 times that of the heavy jet. The sound speed goes as the square root of the temperature, so the same Mach number in the two jets leads to the difference of ~ 31.6 in the actual velocities. This also means that the kinetic luminosity ρv_z^3, has a net increase of 31.6 in going from the heavy jet to the light jet.

The final point we make is simply to reemphasize the existence of enormous jumps in pressure along the jet axis. Note that while the shocks are very strong, leading to jumps in pressure as high as 500, the rarefactions immediately following the shocks are equally strong. This means that the knots are very isolated, with high contrast against the mean pressure background of the jet. This is particularly important for the astrophysical jets, in which the synchrotron emission scales roughly as p^2 (see paper IV).

We turn now to the cut across the beam at $Z = 47$, fig. 12b. The major contrast with the heavy beam in fig. 10b is that the light beam has a low density cocoon with negative velocity surrounding it. This means (compare density plots in figs. 10b and 12b) that the supersonic beam is always surrounded by lighter material, whether the inlet density ratio of the beam to the ambient material is high or low. This contributes strongly to the beam stability. Once again we see that a linearized stability analysis of a *naked* light beam would not have had the correct self-consistent background,

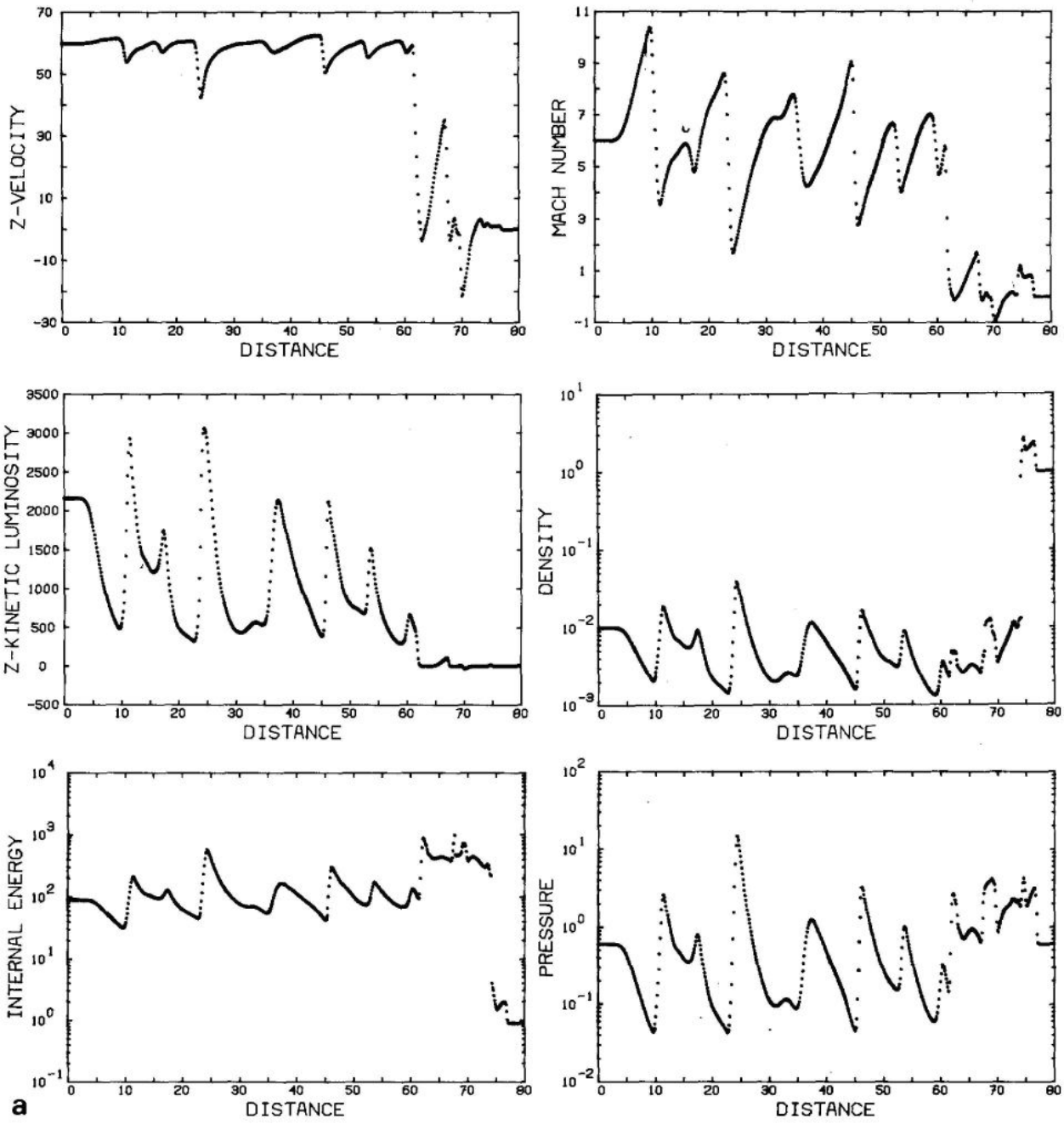


Fig. 12a.

i.e. one could never have guessed that one should surround it by an even lighter cocoon. This is another illustration of the importance of using supercomputers to solve the full problem.

In summary, the cocoon makes the jet structure much wider than in the dense beam case. However, because the cocoon is so light, the kinetic luminosity profile is even sharper and narrower than in the dense beam case. That is, although there is energy transport backward along the cocoon, it is negligible compared to that energy carried forward by the beam. The gas in the cocoon

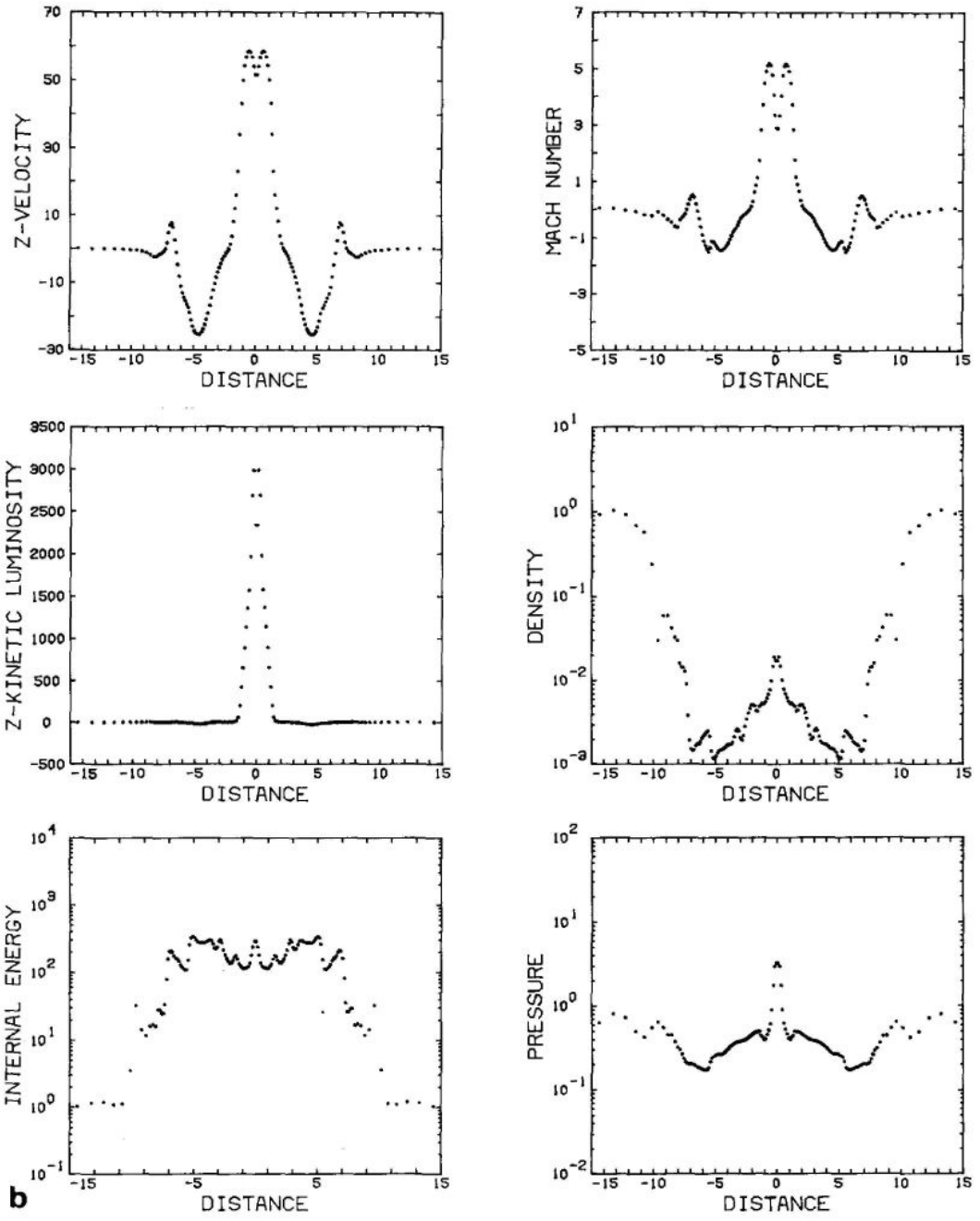


Fig. 12. Same as fig. 10, except for the Mach 6, density ratio 0.01 jet. Note that the spacing between the cocoon-dominated shocks is much larger than for the mode-dominated shocks. Here the spacing represents the distance between shed vortices in the cocoon. The jumps in pressure across shocks along the axis can be as great as 300. Even so, the beam is not disrupted. The beam diameter is roughly constant as can be seen in the kinetic luminosity plot across the jet. The wide return flow (negative velocity) in the cocoon can be seen in the V plot across the jet.

is shocked to higher temperatures by the terminal shock, but then it is adiabatically expanded and cooled in the larger volume of the cocoon. Thus, the resulting temperature profile is fairly constant across both the beam and cocoon (internal energy plot in fig. 12b), and much higher than in the ambient medium. Again, large transverse pressure gradients exist in both the beam and in the cocoon. Finally, note that the interface tracer (solid line in the density plot in fig. 7) locates the boundary between the jet gas in the cocoon and the ambient medium gas. It is much sharper than the density or temperature profiles across this boundary in fig. 12b.

5.3. *External shocks*

In both the dense (fig. 9) and light (fig. 10) jets, we see that there are shocks *external* to the supersonic beam. However, the dense jet drives the shocks directly into the *ambient medium*, whereas the light jet has its external shocks *inside of the cocoon*. In astrophysical jets, these will have very different observational characteristics. The radio emission from astrophysical jets is caused by the synchrotron process of shocked electrons spiraling around local magnetic fields. The magnetic field is carried along the jet from inside the galaxy. This means that in the cocoon the field will be present where the shocks are, thus producing a diffuse emission from large portions of the cocoon. The dense jets, on the other hand, do not possess a cocoon, and therefore the magnetic field will not be present where the external shocks are. These shocks will thus be invisible, unless the shocks compress the ambient gas enough to ionize it and produce emission lines. This provides a means, in principle, of distinguishing between dense and light jets observationally.

There is a spurious external shock in several of our runs (the Mach number 6, density ratios 1.0 and 0.1 and Mach number 12, density ratio 10.0). This is caused by the reflection of the bow shock off the outer constant pressure boundary condition. Only in the Mach 6, density ratio 1.0 case does it have a significant impact on the solution. There the effect is to give a finite amplitude pressure perturbation to the beam, thereby guaranteeing the development of internal shocks. However, since the beam was already long enough to have the mode-dominated shocks anyway (see density ratio 10.0 jet above it), this is not a major contribution. These unwanted external shocks are not a feature solely of computational aerodynamics. In wind tunnels, such reflected shocks can occur from apparatus in the tunnel (see, e.g., fig. 271 in Van Dyke [35]). The important lesson here is that with computer graphics, such numerical features can be easily identified in the solution and be taken into account.

5.4. *The terminal shock system*

Finally, we come to the most important shock system in the problem, the one which terminates the supersonic beam at the head of the jet. As mentioned in section 4, Blandford and Rees [22] concluded on the basis of simple reasoning that there must be bow shock in the ambient medium, a contact discontinuity between the ambient gas and the beam gas, and a terminal shock in the beam gas. However, figs. 6, 7, and 8 demonstrate that the nature of these three discontinuities is much more complicated than this simple picture suggests.

An important discovery of our computer simulation is that the structure and shape of the terminal shock and the contact discontinuity are highly time dependent. Fig. 4 shows how the head of the jet changes shape as the jet advances. Fig. 2 of paper IV shows the detailed dynamics of the contact for the Mach 6 jet with a density ratio of 0.1. As part of this time dependence, the terminal shock changes its pattern dramatically. Figs. 3–6 in paper IV give high resolution views of the terminal shock at four times in the history of this single jet evolution.

We will describe one example of a terminal shock configuration to illustrate the complexity of this dynamic structure. Consider the Mach 6, den-

sity ratio 0.01 jet. From the entropy plot of the final state in fig. 4, one sees that the beam bifurcates as it approaches the head of the jet. The red color indicates high entropy gas, so we can tell that the center part of the beam was shocked more strongly (dark red) than the outer part of the beam (orange). This is confirmed by noting that the kinetic luminosity contours in fig. 13 also bifurcate in the same way. The velocity vectors in fig. 13 show that the beam gas is almost brought to rest near the axis, but continue at high speed in the outer part of the beam. From fig. 11a, one can see a characteristic triple point shock configuration of incident shock, Mach disk shock and reflected shock is responsible for this phenomenon. The strong Mach disk stops the axis gas, while the off-axis beam flow goes through the weaker and oblique incident and reflected shocks. The reflected shock also deflects the flow upward, causing the bifurcation.

The axis flow then accelerates until its speed is the same as the off-axis flow (fig. 13). At this point, a strong transverse shock stops all forward flow. In fig. 4, this causes the yellow in the bifurcation to jump to red, the kinetic luminosity contours stop abruptly (fig. 13), and a high pressure disk (yellow/red in fig. 7) forms. The flow now diverts upward with most of the gas being turned into the cocoon (fig. 13). However, a portion of the gas is trapped in the beam "cap" at the head of the jet in a clockwise rotating vortex ring. Note that this causes the gas to flow *backward* on and near the axis (see also the V_z plot in fig. 12a). Thus, the beam gas is actually *colliding* from both sides (in

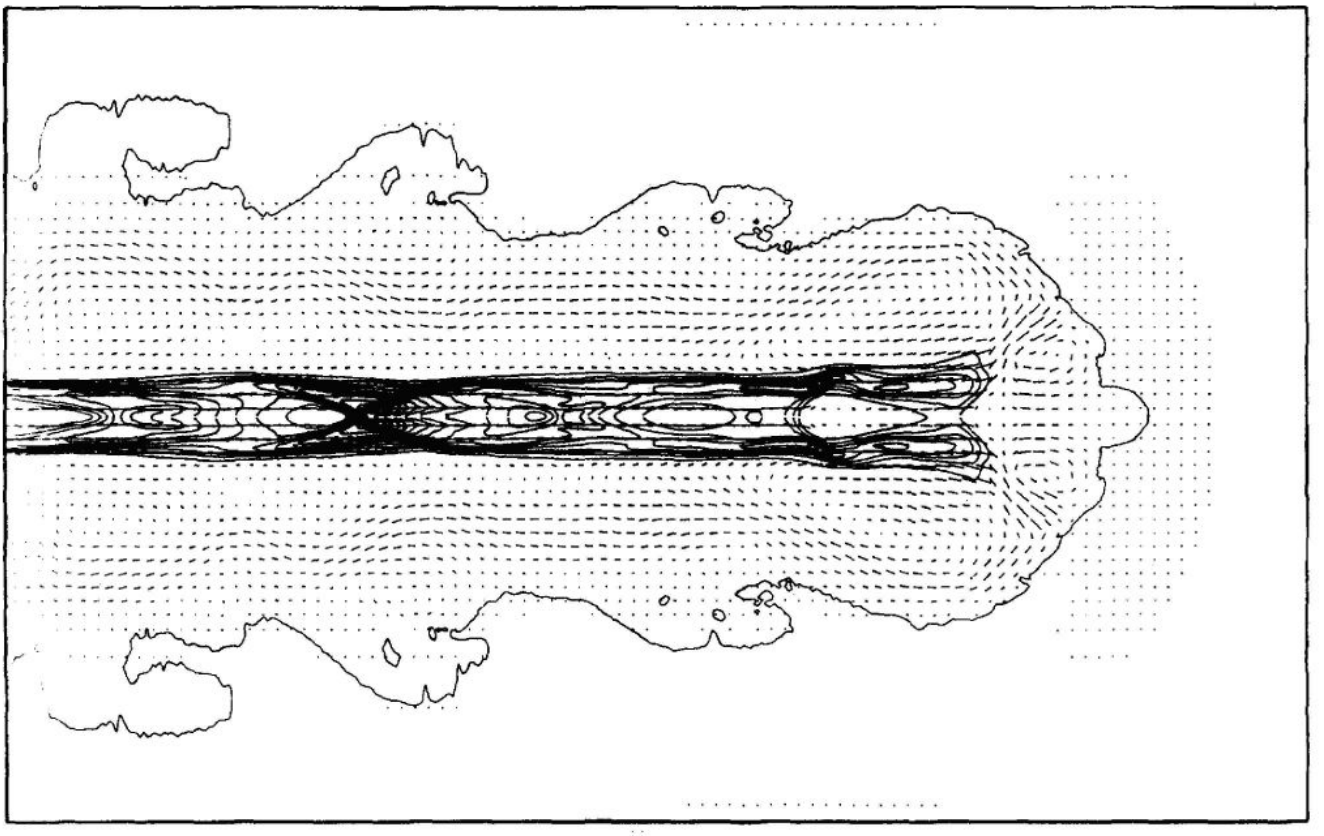


Fig. 13. The velocity field of the head of the Mach 6, density ratio 0.01 jet. The short line segments give the direction of the local velocity, with their length proportional to the speed. The contour lines are of kinetic luminosity (ρV_z^3). One can see a number of vortices embedded in the flow.

the ambient medium frame) of the strong terminal shock.

Finally, the gas which flows into the cocoon froms a large counterclockwise rotating vortex directly over the bifurcation. This flow produces a low pressure (blue in fig. 7) region which is responsible for creating the underexpanded triple point Mach disk configuration in the first place (see detailed discussion in paper I). This vortex is just about to be shed in place, while the beam head advances forward (see shedding sequence in fig. 4 of paper I). The vortex will then swirl the cocoon interface around, creating another large surface wave like the three already present in fig. 13. As the vortex separates from the head of the beam and slowly moves backward, it causes the underlying shock structure to also move backward, thus explaining the backward moving pressure features seen in the spacetime of fig. 11b.

Since the nature of the terminal shock system is discussed in great detail in papers I and IV, we will not go into any more depth here. We can summarize by saying that the patterns at the end of the jet, seen in the pressure plots in figs. 6, 7, and 8, are caused by this time varying terminal shock system. Note that this can cause either single "hot spots" as in the Mach 12, density ratio 0.1 case, or multiple "hot spots" as in the Mach 12, density ratio 0.01 case. Furthermore, these multiple hot spots can be off-axis as seen in fig. 6, paper IV.

6. Interfaces in axisymmetric jets

There are three major interfaces in an axisymmetric jet. The primary one is the interface between the supersonic beam and its surrounding medium. The next one is the contact discontinuity between the jet gas and the ambient medium at the head of the jet. Finally, there is the interface between the cocoon and the ambient medium, in those cases where the jet has a major return flow. All these interfaces are unstable to either Kelvin–Helmholtz or Rayleigh–Taylor instabilities. It has been a matter of great concern to astrophysicists as to whether these instabilities, in their nonlinear limit, can pinch off or otherwise destroy the jet. These are essentially nonlinear coupled processes, whose elucidation requires detailed numerical simulation.

Our computer code includes an interface tracker (described in paper V) which follows the position of the interface between jet gas and ambient gas. In a naked beam, this is the interface along the supersonic beam, because there is no significant backflow of shocked beam gas. In the jets with large backflow, the interface is between the cocoon gas and the ambient gas. In this latter case, the boundary between the beam and cocoon is not followed by the interface tracker, but must be determined self-consistently by the hydrodynamics. The sharpness of the interfaces can be seen in the density plots of figs. 6, 7, and 8 for the cases of naked beams and cocoon-dominated jets.

6.1. *The beam/cocoon interface*

If the supersonic beam were to pinch off then the jet could not be used to transport the energy, mass and momentum to the great distances required by the observations of astrophysical jets. As mentioned in the last section, pinching modes in supersonic beams saturate in internal shocks. On the upper side of the dashed straight line in the parameter space plot (fig. 5), we find that the shocks are planar and the beam disrupts by severe necking down. On the lower side, the shocks are biconical and the beam is in general not disrupted. In this section, we will examine what the existence of these shocks do to the interface between the beam and its surroundings.

The location of that interface is given directly by our interface tracker in the case of the high density jets. In the color density plot for the Mach 6, density ratio 10 jet, fig. 7, one can see that with the biconical shocks fully developed, the beam interface is modulated by a periodic oscillation.

That oscillation has saturated at a small enough amplitude that the beam does not pinch off. This behavior of the interface is typical of naked beams in the portion of parameter space (fig. 5) which is dominated by biconical internal shocks. It is verified by our higher resolution "clean" runs in fig. 9c of paper III.

The behavior of the interface is radically different in the ordinary mode region *above* the dotted line in fig. 5. An example of such a jet which we have studied in some detail is the Mach 1.5, density ratio 1 jet. As the head of the jet moves along (fig. 10b of paper I), a large vortex above the head efficiently entrains material across the equal density interface. After the jet has moved off the right side of our grid, the beam interface develops large "breaking waves" (fig. 14 of paper I), which not only entrain material in the beam, but also breaks it up into a series of subsonic/supersonic pieces. A high resolution run (figs. 9a,b of paper III) graphically shows how the Kelvin–Helmholtz waves grow as they propagate downstream, leading to greater and greater necking down of the beam. The planar shocks interior to the beam are clearly associated with these necking down regions. Another example is the Mach 3, density ratio 10 jet shown in fig. 6. Again the necking down is quite clear. We expect these pinched jets to rapidly become 3-D unstable after the first wave or two on the interface, much like the round turbulent subsonic jets pictured in laboratory studies (Dimotakis, et al. [30]).

Finally, we come to those low density, high Mach number jets which have extensive cocoons. Here an effective way to visualize the beam interface is to plot the kinetic luminosity, ρv_z^3, since there is an abrupt jump in both density and velocity at the beam/cocoon interface. We did this for all our jets in paper II. There one can see that the beam has the same sort of small amplitude oscillations as the naked beams exhibit. There is no tendency for the beam to pinch off. In fig. 13, we plot this same quantity for a blow-up of the front end of the Mach 6, density ratio 0.01 jet. Again, one can see the oscillations in the beam/cocoon interface.

6.2. *The working surface interface*

We used the term "working surface", coined by Blandford and Rees [22], for the head of the jet where the beam gas is brought to rest, relative to the contact discontinuity which separates the beam gas from the ambient gas. Ahead of this contact sits the bow shock in the ambient medium. As mentioned above, we have found the shape of this contact to be time dependent. We make a cautionary warning that this time dependence may be accentuated by the assumed axisymmetry of the calculation. This forces the intersection of the symmetry axis and the contact to be a stagnant point and therefore be more unstable than it would be in a 3-dimensional jet. However, there is some evidence from laboratory studies of the dynamics of supersonic fluid jets, that the head of the jet does suffer oscillations (Brad Sturtevant, Cal. Tech., private communication). Although the working surface accelerates and decelerates in time, as can be seen by its oscillating trajectory in spacetime in fig. 11, the interface does not develop a strong Rayleigh–Taylor instability.

As described in section 5.4., the head of the jet exhibits a highly nonlinear coherent self-excited structure which combines shocks, interfaces and patterns in an intimate way. Our studies have opened up a panorama of complicated dynamic phenomena.

6.3. *The cocoon interface*

After the supersonic beam gas is stopped in the rest frame of the terminal shock, it is pushed to the side. If the beam gas is dense enough (density ratio 10), it can maintain its forward momentum in the rest frame of the ambient gas. Thus, the waste gas rides along with the head of the jet. If the beam gas is just as dense as the ambient gas (density ratio 1), then it is brought to rest in the frame of the ambient gas. This leads to a thin sheath which is laid down around the beam as the beam propagates. As the beam density is lowered below the ambient density, the return flow begins to move

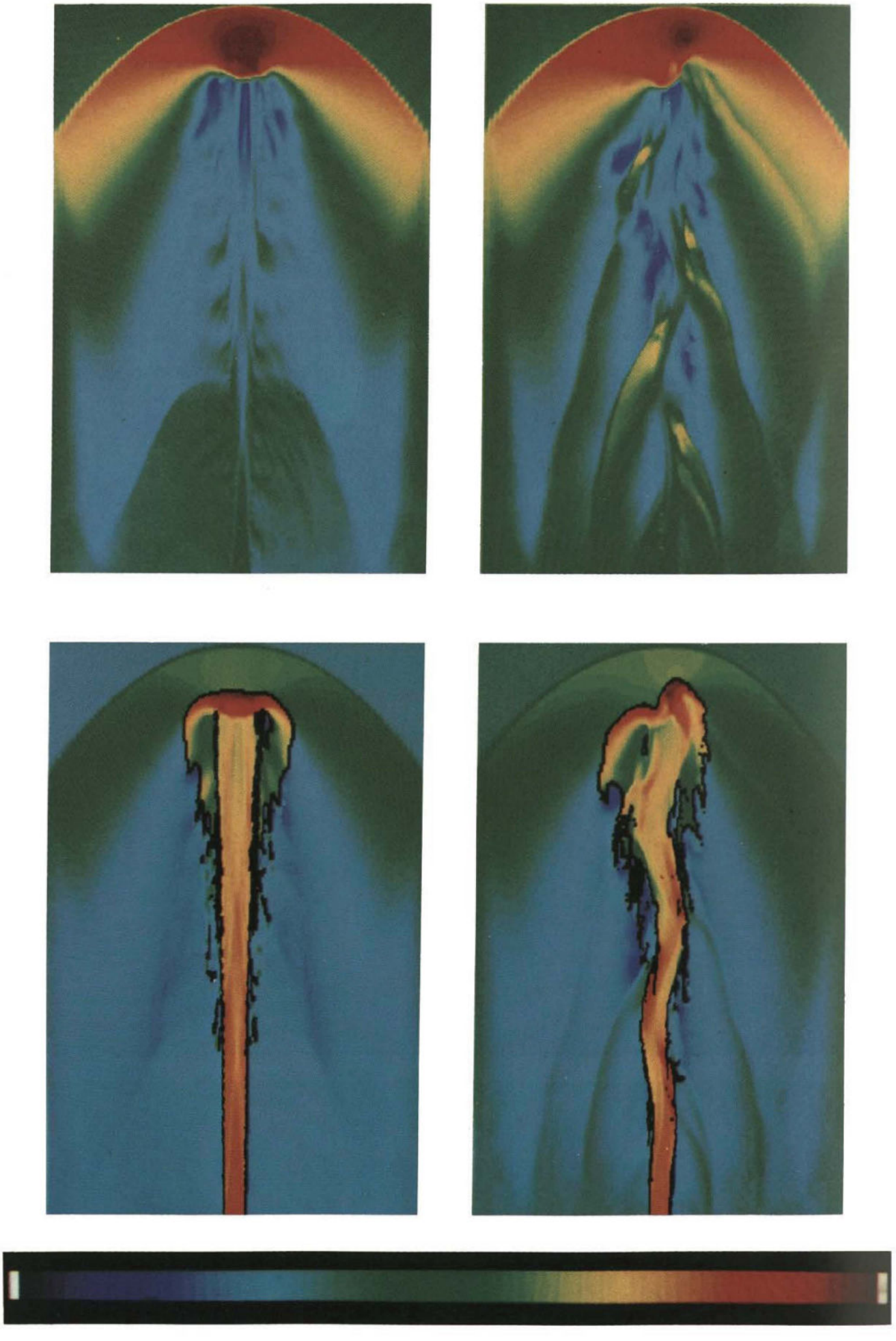


Fig. 14 (for caption see text on opposite page).

Captions to color plates

Fig. 4. The time evolution of an axisymmetric jet. The plane of the picture contains the symmetry axis of the jet. Gas is continuously introduced from a circular inlet at the left, with an internal Mach number of 6, a density 0.01 times the ambient density, and a pressure equal to the ambient density. The quantity plotted is entropy. It is represented by 73 shades of color, each color representing an equal logarithmic interval between the maximum and minimum value of the entropy. The order of the colors is the same as the spectrum, see color bar in fig. 6. Dark blue is the minimum and bright red is the maximum. The jet is divided into a forward moving beam and a surrounding backward moving cocoon. The interface between the cocoon and the ambient medium has nonlinear Kelvin–Helmholtz waves on it. Note that these are roughly stationary in space as the beam advances. The swirls in the red region of the cocoon reveal large scale vortices which mix low entropy material from the ambient medium into the cocoon, changing its color from red to green.

Fig. 6. The Mach 3 jets. Density fields are shown on the left page (fig. 6a) for beam ambient medium density ratios of 10.0, 1.0, and 0.1 (from top to bottom, respectively). Corresponding pressure fields are given on the right page (fig. 6b). The heavy dark line in the density plot represents the interface between the jet gas and the ambient gas. The standard color bar is given at the bottom of the density plots. Note that the top jet almost pinches itself off. The lower two jets have periodic internal shocks where the pressure color changes abruptly from blue to red.

Fig. 7 The Mach 6 jets. Same as in fig. 6, except that a density ratio 0.01 jet is also included at the bottom of the page. Note that the lower two jets have extensive cocoons, which causes the internal shocks to be much more widely spaced. The pressure plots show, in the middle two jets, that the bow shock reflects off the constant pressure boundary at the edge of the grid. The interface of the density ratio 1.0 jet has a periodic set of nonlinear Kelvin–Helmholtz waves on it.

Fig. 8. The Mach 12 jets. Same as in fig. 7. Those jets with naked beams (the top two) do not yet show strong internal shocks because they are shorter than the growth length for the reflecting mode perturbation to go nonlinear. If they are evolved to twice this length, they will develop internal shocks similar to fig. 7. The bottom two do have some internal shocks because they are driven by finite amplitude pressure variations in the cocoon.

Fig. 14. A Mach 6, density ratio 10.0 slab jet. The two images on the left are from a run where no perturbation was applied to the inlet flow. The two on the right are the same inlet conditions except that a periodic wiggle is applied to the inlet velocity. The bottom figures are density plots, the top two are pressure plots. Note the similarity of the left jet with axisymmetric Mach 12, density ratio 10 jet in fig. 8. No internal shocks have developed because the jet is shorter than its growth length. The asymmetric alternating shocks which develop in the right run will soon cause the jet to kink sharply and break up.

backward relative to the ambient medium, until at a density ratio of 0.01 it has become supersonic in the ambient medium rest frame. This causes a well inflated cocoon to surround the beam. All three of these cases can be clearly seen in figs. 6, 7, and 8.

In the case of the low velocity backflow, e.g. the Mach 3, density ratio 0.1 jet, the overturn time of the vortices in the cocoon is comparable to the timescale for the head of the jet to advance a vortex width. This is accompanied by efficient entrainment of the denser ambient medium gas into the cocoon. This process is shown at early times in the pair of pictures in fig. 9 of paper I. The long term result is that the cocoon can only stay inflated near the head of the jet, forming a lobe as seen in fig. 6. Those cocoons which have a supersonic velocity relative to the ambient medium, have a much more stable interface. However, even in the Mach 6, density ratio 0.01 case, the embedded vortices in the cocoon ultimately cause entrainment of ambient medium gas. This can be seen very clearly in the entropy sequence for this jet in fig. 5. Note that the entropy decreases (color goes from red to yellow to green), due to mixing, the further one gets from the head of the jet.

The embedded vortices, clearly seen in the velocity vector field in fig. 13, are caused by the periodic vortex shedding mentioned in the last section. Note the string of regularly spaced vortices which distort the cocoon interface in the Mach 6, density ratio 1 plot in fig. 7. This brings to mind the regularly spaced vortices which are often seen along shear layers in incompressible flows.

7. Nonaxisymmetric jets

It is clear that jets in the real world do not maintain exact axisymmetry forever, even if they start with axisymmetric initial conditions. There are two reasons for this. First, the environment in which the jet propagates may impose a finite nonaxisymmetric pressure gradient on the jet. Second, axisymmetric jets are unstable to nonaxisymmetric perturbations and these can exponentiate infinitesimal disturbances to finite ones. In an axisymmetric code, neither of these effects can occur. To investigate them we ran several slab symmetric jets. These are jets which are infinite in extent in one of the directions perpendicular to propagation, but finite in the other perpendicular direction. This symmetry is a good approximation to jets which issue from a thin slit orifice, such as the laboratory jet shown in fig. 1.

In figs. 14a, b, we show the density and pressure plots for a Mach 12, density ratio 10 slab jet with no perturbation applied. It has propagated about 2/3 as far (in units of the inlet diameter) as the same parameter axisymmetric jet shown in fig. 8. The two jets are remarkably similar in structure. In particular, both jets have internal and external shocks, with the highest pressure in the region between the terminal shock and the bow shock. However, as mentioned in section 5.1., the Mach 12 jet has not had time enough for the instabilities to grow to nonlinear strength. When we evolved further the axisymmetric jet (fig. 11 in paper III), we found that the reflecting mode biconical shocks developed.

In the slab symmetric case, there are two competing instabilities, the ones which are symmetric about the midline of the slab (Xs) and the ones which are not symmetric (kinks). Which of these wins depends on the strength of the initial perturbations in both modes. In the laboratory jet shown in fig. 1, the symmetric mode clearly wins. This is because, although the jet pressure was fairly closely matched to the ambient pressure, a mismatch of a few percent is likely. Since the mismatch is the same above and below the slab, it exerts a symmetric disturbance on the jet causing the beautiful crisscrossed shocks seen in fig. 1. Just as with the biconical axisymmetric internal shocks, these symmetric shocks do not seem to interfere with the jet propagation.

To illustrate the other extreme, we did a numerical experiment in which we applied a few percent nonsymmetric perturbation to the slab jet inlet. In detail, we wiggled the incoming flow (Mach 12, density ratio 10 as above) up and down through

0.05 radians, conserving speed, at a frequency corresponding to twice the most unstable nonsymmetric mode. In figs. 14c, d, one sees the resulting density and pressure plots at the same time as in figs. 14a, b. As in the symmetric laboratory case (fig. 1), the perturbations immediately saturate into shocks, because of the finite amplitude of the perturbation. However, here the flow is severely affected, with the beam kinking more and more with time, ultimately disrupting the beam. The high pressure and density "knots" after the shocks are no longer collinear with the beam, but instead alternate from side to side. As in the late time axisymmetric Mach 12 jet, the internal and external shocks are intimately coupled. The oscillations in the jet interface, caused by the internal shock systems, in turn cause shock systems in the external medium. Other numerical investigations of kink instability, mainly in periodic flow boundary conditions, have been reported (see e.g. Tajima and Leboeuf [31], Nepveu [32], and Woodward [33]), which show in more detail the structure of these shocks.

8. Conclusions

We started this paper by observing the real world of supersonic jets. There is evidence that in the laboratory, in aerodynamics, and in astrophysics, supersonic jets exist that are nearly axisymmetric or slab symmetric for many jet diameters. These jets range in length from centimeters to millions of light years. Almost all of these jets exhibit knots of emission inside of their beams. There was clear evidence in the laboratory case that these knots are caused by periodic shock wave systems. Although in the laboratory and in aerodynamics one is usually not interested in the transient behavior of the jet head boring through the ambient medium, it seems clear that one is seeing the astrophysical jets in just such an evolution. These cosmic jets seem to require strong terminal shocks to explain their hot spots near the head of the jet.

These patterns, reoccuring over such enormous length scales, indicate that some fundamental scale-free nonlinear hydrodynamics is at work here. To investigate this possibility we undertook to use a supercomputer to simulate these flows. The equations integrated were the basic inviscid equations of hydrodynamics (continuity equation, adiabatic energy equation, and Euler equation). Because these equations have no other physics in them, they are scale-free and their solutions should apply to laboratory or astrophysical jets equally well. We fixed a uniform ambient medium and then ran a two-parameter set of jets through it. We realize that other physics (heating and cooling, phase changes, magnetic fields, etc.) may break the scale invariance in some particular jets and we are extending our basic analysis to incorporate such effects.

We found that all jets develop internal shock waves if they propagate to a distance long enough for perturbations to grow to nonlinear amplitude. In the axisymmetric case, there are two regimes of shock physics. One in which the shock waves are planar and disrupt the beam and one in which the shocks crisscross the beam and do not disrupt it. The boundary between the two regimes coincides well with the boundary found (Cohn, [29]) in perturbation theory between ordinary Kelvin–Helmholtz pinching modes and the higher order reflecting modes.

These shocks occur at regular intervals along the beam, causing enormous jumps in pressure internal to the beam. A spacetime diagram of the knots reveals two qualitatively different dynamical patterns. The one is that of closely spaced knots propagating downstream with the velocity of the leading bow shock. The other is that of the slow backward drift of widely spaced knots with a more chaotic appearance. The difference between these two behaviors was traced to the other major pattern in supersonic jets: the existence of a cocoon of return gas flow around fast light jets. If there is such a cocoon, the vortices in the return flow drive the instabilities in the beam and produce the second type of spacetime diagram. If the beam is

naked, then the knots seem to develop from the free growth of perturbations to nonlinear strength, producing the first type of spacetime diagram.

The terminal shock physics was found to be highly time dependent and fairly complex. However, almost all features of the flow can be understood in terms of simple concepts from textbooks on supersonic flow. The strong shock at the end of the jet is likely to explain the hot spot phenomenon in astrophysical jets. There is a shedding of vortices and the development of large breaking waves on the cocoon/ambient medium interface.

Our slab jet calculations indicated that such jets can propagate for many jet diameters if they are not disturbed. However, if hit with a nonsymmetric finite amplitude perturbation, they go into a kinking instability, which ultimately destroys the beam. This produces alternating shock waves along the beam, more widely spaced than in the free axisymmetric jet case.

In the real world, the ability of jets to propagate to large distances without destroying themselves is observed. However, ultimately many such jets begin to wiggle and soon end. Thus, we expect that fully three-dimensional computer simulations will be necessary to model these jets. These calculations await larger and faster computers. Nonetheless, much of the basic physics of the shocks, patterns, and interfaces of supersonic jets seems to come out of our two-dimensional models. A crucial tool of analysis for computer simulations are the color images that we displayed herein. One of the great challenges for tomorrow's calculations is how to visualize the basic physics of time dependent three-dimensional flows.

Acknowledgements

We wish to thank the Los Alamos Center for Nonlinear Physics for financial support to attend the conference. The National Science Foundation (grants number PHY 80-01496 and PHY 83-08826) and the Alfred P. Sloan Foundation provided partial support for one of us (LS). We are particularly grateful to Norman Zabusky for his clarifying and encouraging remarks.

References

[1] E. Mach and P. Salcher, Wien. Ber. 98 (1889) 1303.
[2] L. Prandtl, Essentials of Fluid Dynamics (Blackie and Son, London, 1952).
[3] R. Landenburg, C.C. Van Voorhis and J. Winckler, Phys. Rev. 76 (1949) 662.
[4] F.W. Anderson, Orders of Magnitude, NASA Special Pub. (1981) 4403.
[5] J. Wormhoudt, and V. Yousefian, J. Spacecraft and Rockets 19 (1982) 4, 382.
[6] R. Mundt, and J.W. Fried, Submitted to Ap. J. Letters (1983).
[7] B. Margon, Science 215 (1982) 247.
[8] S. Tapia, G. Jacoby, H.R. Butcher, E.R. Craine and H.S. Stockman, submitted to the Astrophysical Journal (1983).
[9] M.L. Norman, L. Smarr and K.-H.A. Winkler, To appear in Numerical Astrophysics: A Festschrift in Honor of James R. Wilson, J. Centrella, R. Bowers, J. LeBlanc and M. LeBlanc, eds., (1983b), (paper III).
[10] R.D. Blandford, to appear in Numerical Astrophysics: A Festschrift in Honor of James R. Wilson, J. Centrella, R. Bowers, J. LeBlanc and M. LeBlanc, eds., (1983).
[11] M.D. Smith, M.L. Norman, K.-H.A. Winkler and L. Smarr, "Hot Spots in Radio Galaxies: A Comparison with Hydrodynamics Beam Cap Simulations", submitted to Monthly Notices Roy. Astron. Soc. (1983), (paper IV).
[12] R.A. Perley, A.H. Bridle and A.G. Willis, Submitted to the Astrophysical Journal, (1983).
[13] G. Miley, in "Astrophysical Jets", A. Ferrari and A.G. Pacholczyk, eds., (Reidel, Dordrecht, 1983).
[14] E.B. Fomalont, in Astrophysical Jets, A. Ferrari and A.G. Pacholczyk, eds., (Reidel, Dordrecht, 1983).
[15] R.H. Sanders, Ap. J. 266 (1983) 73.
[16] G. Birkoff, SIAM Review 25 (1983) 1.
[17] N. Zabusky, J. Comp. Phys. 43 (1981) 195.
[18] M.L. Norman and K.-H.A. Winkler, in Astrophysical Radiation Hydrodynamics, M.L. Norman and K.-H.A. Winkler, eds., (1984), (paper V).
[19] M.L. Norman, L. Smarr, K.-H.A. Winkler and M.D. Smith, Astron. Astrophys. 113 (1982) 285 (paper I).
[20] M.L. Norman, K.-H.A. Winkler and L. Smarr, in Astrophysical Jets, A. Ferrari and A.G. Pacholczyk, eds., (Reidel, Dordrecht, 1982). (paper II).
[21] K.-H.A. Winkler, in Astrophysical Radiation Hydrodynamics, M.L. Norman and K.-H.A. Winkler, eds., (1984) (paper VI).
[22] R.D. Blandford and M. Rees, Mon. Not. Roy. Astr. Soc. 169 (1974) 395.
[23] P.E. Hardee, Ap. J. 234 (1979) 47.
[24] P.E. Hardee, Ap. J. 257 (1982) 509.
[25] P.E. Hardee, Ap. J. 269 (1983) 94.

[26] A. Ferrari, E. Trussoni and L. Zaninetti, Astron. Astrophys. 64 (1978) 43.
[27] A. Ferrari, E. Trussoni, and L. Zaninetti, Mon. Not. Roy. Astr. Soc. 196 (1981) 1054.
[28] T.P. Ray, Mon. Not. Roy. Astr. Soc. 196 (1981) 195.
[29] H. Cohn, Ap. J. 269 (1983) 500.
[30] P.E. Dimotakis, R.C. Miake-Lye and D.A. Papantoniou, preprint GALCIT FM82-01 of the Graduate Aeronautical Laboratories of Cal. Tech. (1982).
[31] T. Tajima, and J.N. Leboeuf, Phys. Fluids 23 (1980) 884.
[32] M. Nepveu, Astron. Astrophys. (1982).
[33] P.R. Woodward, Bull. Amer. Astron. Soc. 14 (1982) 4, 810.
[34] M.D. Smith, L. Smarr, M.L. Norman and J.R. Wilson, Ap. J. 264 (1983) 432.
[35] M. Van Dyke, An Album of Fluid Motion (Parabolic Press, Stanford, CA, 1982).